U.S. DEPARTMENT OF COMMERCE
National Technical Information Service

PB-269 604

Studies of Circulation and Primary Production in Deep Inlet Environments

Washington Univ, Seattle Dept of Oceanography

Prepared for

Corvallis Environmental Research Lab, Oreg Marine and Freshwater Ecology Branch

Apr 77

TECHNICAL REPORT DATA

(Please read Instructions on the reverse before completing)

1. REPORT NO. EPA-600/3-77-085	2.
3. RECIPIENT'S ACCESSION NO.	
4. TITLE AND SUBTITLE "Studies of Circulation and Primary Production in Deep Inlet Environments."	5. REPORT DATE April 1977
	6. PERFORMING ORGANIZATION CODE
7. AUTHOR(S) Dr. Donald F. Winter	8. PERFORMING ORGANIZATION REPORT NO.
9. PERFORMING ORGANIZATION NAME AND ADDRESS Department of Oceanography University of Washington Seattle, WA 98195	10. PROGRAM ELEMENT NO. 1BA608
	11. CONTRACT/GRANT NO. R-801320
12. SPONSORING AGENCY NAME AND ADDRESS U.S. Environmental Protection Agency - Corvallis Corvallis Environmental Research Lab 200 S. W. 35th Street Corvallis, Oregon 97330	13. TYPE OF REPORT AND PERIOD COVERED Final Report, 1973-1976
	14. SPONSORING AGENCY CODE EPA/600-02

15. SUPPLEMENTARY NOTES

None

16. ABSTRACT

This report summarizes the results of a three-year grant from the U.S. Environmental Protection Agency to investigate various aspects of circulation dynamics and primary production in a deep inlet environment. Throughout the course of the research, special attention has been given to Puget Sound, Washington, although many of the findings are applicable to other deep inlet waters.

The several tasks undertaken during the course of the project fell into three general categories:

1) Numerical modeling of gravitational convection and tidal motions in deep estuaries.

2) Hydraulic model studies of tidal circulation patterns and dye dispersal characteristics in Puget Sound.

3) Numerical modeling of primary production in a deep inlet (in particular, the deep central basin of Puget Sound).

17. KEY WORDS AND DOCUMENT ANALYSIS

a. DESCRIPTORS	b. IDENTIFIERS/OPEN ENDED TERMS	c. COSATI Field/Group
ecosystem modeling hydraulic modeling circulation diffusion fiords	estuaries modeling	08A 08C 08J 20D

18. DISTRIBUTION STATEMENT Release to public	19. SECURITY CLASS (This Report) Unclassified	21. NO. OF PAGES 110
	20. SECURITY CLASS (This page) Unclassified	22. PRICE A06 - A01

EPA Form 2220-1 (9-73)

EPA-600/3-77-048
April 1977

PB 269 504

Ecological Research Series

REPRODUCED BY
NATIONAL TECHNICAL
INFORMATION SERVICE
U.S. DEPARTMENT OF COMMERCE
SPRINGFIELD, VA. 22161

RESEARCH REPORTING SERIES

Research reports of the Office of Research and Development, U.S. Environmental Protection Agency, have been grouped into nine series. These nine broad categories were established to facilitate further development and application of environmental technology. Elimination of traditional grouping was consciously planned to foster technology transfer and a maximum interface in related fields. The nine series are:

1. Environmental Health Effects Research
2. Environmental Protection Technology
3. Ecological Research
4. Environmental Monitoring
5. Socioeconomic Environmental Studies
6. Scientific and Technical Assessment Reports (STAR)
7. Interagency Energy-Environment Research and Development
8. "Special" Reports
9. Miscellaneous Reports

This report has been assigned to the ECOLOGICAL RESEARCH series. This series describes research on the effects of pollution on humans, plant and animal species, and materials. Problems are assessed for their long- and short-term influences. Investigations include formation, transport, and pathway studies to determine the fate of pollutants and their effects. This work provides the technical basis for setting standards to minimize undesirable changes in living organisms in the aquatic, terrestrial, and atmospheric environments.

This document is available to the public through the National Technical Information Service, Springfield, Virginia 22161.

EPA-600/3-77-049
April 1977

STUDIES OF CIRCULATION AND PRIMARY PRODUCTION IN DEEP INLET ENVIRONMENTS

by

Donald F. Winter
University of Washington
Seattle, Washington 98195

Grant No. R-801320

Project Officer

Richard J. Callaway
Marine and Freshwater Ecology Branch
Corvallis Environmental Research Laboratory
Corvallis, Oregon 97330

CORVALLIS ENVIRONMENTAL RESEARCH LABORATORY
OFFICE OF RESEARCH AND DEVELOPMENT
U.S. ENVIRONMENTAL PROTECTION AGENCY
CORVALLIS, OREGON 97330

DISCLAIMER

This report has been reviewed by the Corvallis Environmental Research Laboratory, U.S. Environmental Protection Agency, and approved for publication. Approval does not signify that the contents necessarily reflect the views and policies of the U.S. Environmental Protection Agency, nor does mention of trade names or commercial products constitute endorsement or recommendation for use.

FOREWORD

Effective regulatory and enforcement actions by the Environmental Protection Agency would be virtually impossible without sound scientific data on pollutants and their impact on environmental stability and human health. Responsibility for building this data base has been assigned to EPA's Office of Research and Development and its 15 major field installations, one of which is the Corvallis Environmental Research Laboratory (CERL).

The primary mission of the Corvallis Laboratory is research on the effects of environmental pollutants on terrestrial, freshwater, and marine ecosystems; the behavior, effects and control of pollutants in lake systems; and the development of predictive models on the movement of pollutants in the biosphere.

This report concerns research conducted on a highly complex estuarine (fjord) system as part of an attempt to assist regulatory agencies in their management role. Results of the research have already been put to practical use by federal, state and local government agencies as well as by commercial engineering firms through utilization of computer programs, the reports listed in the appendix, and consultation with the grantees. As such, the work has formed one part of the base upon which criteria and policy decisions are made and revised.

A. F. Bartsch
Director, CERL

ABSTRACT

This report summarizes the results of a three-year grant from the U.S. Environmental Protection Agency to investigate various aspects of circulation dynamics and primary production in a deep inlet environment. Throughout the course of the research, special attention has been given to Puget Sound, Washington, although many of the findings are applicable to other deep inlet waters.

The several tasks undertaken during the course of the project fall into three general categories:

1) numerical modeling of gravitational convection and tidal motions in deep estuaries,
2) hydraulic model studies of tidal circulation patterns and dye dispersal characteristics in Puget Sound,
and 3) numerical modeling of primary production in a deep inlet (in particular, the deep central basin of Puget Sound).

A list of all publications and reports resulting from the project are given in Section 7 of this report.

This report was submitted in fulfillment of Project No. R-801120 by the University of Washington, Seattle, Washington, under the sponsorship of the U.S. Environmental Protection Agency. Work was completed as of March 1976.

CONTENTS

Sections		Page
1	INTRODUCTION	1
2	CONCLUSIONS AND RECOMMENDATIONS	3
3	CIRCULATION MODELING	
	3.1 STEADY GRAVITATIONAL CONVECTION: TWO-LAYER ANALYSIS	7
	3.2 STEADY GRAVITATIONAL CONVECTION: SIMILARITY ANALYSIS	29
	3.3 STEADY GRAVITATIONAL CONVECTION: METHOD OF WEIGHTED RESIDUALS	36
	3.4 PERIODIC TIDAL MOTION IN NARROW INLETS	40
4	HYDRAULIC MODEL STUDIES OF PUGET SOUND	
	4.1 MODEL DESCRIPTION AND LIMITATIONS	46
	4.2 SURFACE TIDAL CURRENTS IN PUGET SOUND	49
	4.3 DYE STREAM DISPERSAL CHARACTERISTICS IN THE PUGET SOUND MODEL	57
	West Point	61
	Elliott Bay	62
	Dredge Disposal Sites	66
5	NUMERICAL MODEL OF PRIMARY PRODUCTION IN PUGET SOUND, WASHINGTON	75
6	REFERENCES	96
7	PUBLICATIONS AND TECHNICAL MEMORANDA	98

FIGURES

No.		Page
1	Sketch of an inlet cross-section (a) and longitudinal section (b), depicting the two major flow zones and illustrating geometrical quantities. The horizontal scale is compressed.	9
2	Sketch of an inlet longitudinal section, illustrating zonal fluid sections used to derive equations of conservation of volume, mass, and horizontal momentum.	9
3	Map of Hood Canal, Washington.	16
4	Bottom profile of Hood Canal, Washington, and salinity isopleth configuration in mid-November 1954.	19
5	Idealization of Hood Canal bottom profile used in model calculation	19
6	Principal drainage basins of Hood Canal.	21
7	Relative cumulative runoff rate in Hood Canal.	21
8	Axial variation of deep and near-surface zone salinity in Hood Canal during October and November.	22
9	Calculated axial variations of mean horizontal current speed (a), zonal depth (b), and upward transport function F_u (c) in Hood Canal for October and November.	24
10	Comparison of measured and calculated isohaline configuration in a longitudinal section of Hood Canal; the data were acquired at the stations shown in the map.	33
11	Comparison of calculated depth profiles of salinity and salinity measurements acquired in May 1966 at a mid-channel station in the central basin of Puget Sound for (a) a relatively high runoff rate: $R_0 = 495$ m^3 sec^{-1} and (b) a moderate runoff rate: $R_0 = 210$ m^3 sec^{-1}. Velocity profiles for the high runoff period are also shown: (c) horizontal component; (d) vertical component.	34
12	Comparisons of salinity profiles throughout Knight Inlet, B.C., as calculated by the weighted residual method and by the two-layer analysis. Axial location is distance upstream of the inner sill.	39

No.		Page
13	Narrow inlet geometry.	41
14	Axial variation of velocity mode amplitudes for model inlet.	41
15	Hydraulic model coverage (outlined by dashed line) and the locations of the dye discharge experiments.	47
16	Hand-drawn replication of part of the tidal mosaic for one stage of the tide; direction and magnitude of surface tidal current is indicated by orientation and length of streamline segments.	50
17	Map of Puget Sound showing the measured model tides; dots on the tide curves correspond to the time of the eight streamline photographs.	51
18	Measured model tide at Seattle; the times correspond to the beginnings of each of the eight streamline photographs.	53
19	Representative spring tides at Seattle (May 1973, days 1 through 10).	58
20	Representative neap tides at Seattle (October 1973, days 2 through 11).	58
21	Dye discharge locations near Seattle; solid triangles are dredge disposal sites.	65
22	Dye discharge locations at two dredge disposal sites in Commencement Bay.	68
23	Dye discharge location at the dredge disposal site near Everett.	72
24	Dye discharge location at the dredge disposal site in Dana Passage.	74
25	Map of Puget Sound.	77
26	Variations of salinity, temperature, density, oxygen saturation, phosphate, silicate, nitrate, chlorophyll a, and carbon uptake rate at Station 1, April to June 1966.	79
27	Variations of salinity, temperature, density, oxygen saturation, phosphate, silicate, nitrate, chlorophyll a, and carbon uptake rate at Station 1, April and May 1967.	80

No.		Page
28	Flow diagram of numerical model showing relationship amongst the several components of the model.	88
29	Comparison of measured and calculated integrated chlorophyll *a* from surface to Secchi disk depth and Secchi disk depth at Station 1 in Puget Sound, April to June 1966; arrows indicate endings of periods of rapidly rising salinity in brackish zone.	90
30	Comparison of measured and calculated integrated chlorophyll *a* from surface to Secchi disk depth and Secchi disk depth at Station 1 in Puget Sound, April and May 1967.	91
31	Comparison of measured and calculated chlorophyll *a* concentrations as functions of depth at Station 1 before, during, and after algal bloom in 1966; dashed lines indicate estimates of 1% light depths.	93
32.	Depth variation of algal flux due to turbulent mixing, upwelling, and sinking for standard run at noon on 28 April 1966.	94

ACKNOWLEDGMENTS

The writer wishes to acknowledge with appreciation the support of this project by the Environmental Protection Agency under Grant No. R801320.

The contributions of all the research collaborators whose names appear as authors in the publication list in Section 7 were essential to the success of this project. Special thanks are due to Dr. Ronald K. Lam and Mr. John H. Lincoln of the Department of Oceanography, University of Washington, who carried out and reported the hydraulic model studies of Puget Sound described in Section 4.

The numerical modeling study of primary production in Puget Sound described in Section 5 was supported in part by the Washington Sea Grant, which is maintained by the National Oceanic and Atmospheric Administration, U.S. Department of Commerce. Funds for the field effort in that study were provided primarily by the United States Public Health Service and later by the Federal Water Pollution Control Administration (Grant WP-00633). Minor assistance was given by the Office of Naval Research, Contract Nonr-477(37), Project NR 083 012, and the U.S. Energy Research and Development Administration, Contract AT(45-1)-2225, TA 36 (RLO-2225-T 36-21).

The two-layer analysis of steady deep inlet flow, as set forth in Section 3.1, is a recent modification of the method developed originally under Grant No. R801320. The procedure described here was developed by Prof. Carl E. Pearson and the author under the auspices of Program Research, Inc., with support from EPA, subsequent to the expiration of Grant No. R801320. However, the modified approach is presented here inasmuch as it represents an improved version of the original method.

Staff assistance in the University of Washington Department of Oceanography is acknowledged in each of the publications, as appropriate. The writer expresses special thanks to Ms. Betty Hardin for typing this report and preparing it for publication.

SECTION 1

INTRODUCTION

In recent years, deep inlet waters have been subject to increasing environmental stress associated with rising population densities and industrial activity. In many areas, these developments have been accompanied by efforts to improve and preserve inlet water quality through the institution of rational water management and utilization programs. Such efforts have a greater chance to succeed if the biological and chemical characteristics of an inlet are known and if the hydrography and water movement can be described in quantitative terms. Although in many respects the research described in this report responds to the general need for such descriptions in deep inlets, special consideration has been given to Puget Sound, Washington, in most phases of the work.

Section 2 of this report summarizes the approach and conclusions in each of three principal categories of the project and presents recommendations of future research directions, where appropriate.

Section 3 presents descriptions of several different numerical models of deep inlet circulation, including time-averaged flow and periodic tidal motions.

Section 4 describes two investigations with the hydraulic model of Puget Sound. One study is concerned with a description of surface tidal current patterns throughout the Puget Sound region. The other deals with dye-stream dispersal characteristics in the model at various locations in the Sound which are sites of potential pollution stress.

Finally, Section 5 presents a summary of field measurements in the central basin of Puget Sound conducted over a period of several years and includes both conventional hydrographic data and measurements related to biological activity. Highlights are also presented of the results of a numerical model

study of the relationship between primary productivity and the hydrodynamic characteristics of a deep inlet environment, as exemplified by the central basin of Puget Sound.

SECTION 8

CONCLUSIONS AND RECOMMENDATIONS

The overall objective of this research has been to investigate various aspects of deep inlet circulation with a view toward improving our ability to represent flow patterns and to explore relationships between circulation and phytoplankton growth (primary production) in a deep inlet environment. The tasks undertaken in pursuit of this general objective fall into three categories: 1) numerical modeling of deep inlet hydrodynamics, 2) hydraulic model studies of tidal circulation patterns throughout Puget Sound, and 3) numerical modeling of primary production in the central basin of Puget Sound, Washington. The principal accomplishments, conclusions, and recommendations in each category are as follows:

1) CIRCULATION MODELING

Circulation in deep, narrow inlets with appreciable freshwater input is generally dominated by two modes: quasi-steady gravitational convection and periodic tidal motion. With regard to the first of these modes, it is characteristic of deep, stratified inlet flow that the most vigorous circulation takes place in a brackish water zone near the surface. During the course of the project, three different types of approximation procedures were used to represent this mode; the techniques included: similarity analysis, a two-layer representation, and a weighted residual approach. Approximate descriptions were obtained for time-averaged or quasi-steady state velocity fields and density distributions. These representations have been applied to inlet segments in Puget Sound and along the coastline of British Columbia. In each case, the procedures used can be adapted to analyze distributions of dissolved and suspended pollutants.

The various steady-state models simulate the gross features of observed time-averaged flow and density distributions where such comparisons have been made. However, none of these models of steady inlet flow (or any other one, for that matter) can be considered entirely satisfactory. Our experience in this

research effort suggests that high priority ought to be given in the future to i) carefully designed field studies with high data resolution in space and time to identify and describe more precisely basic patterns of deep inlet fluid motion and to allow more reliable quantitative descriptions of the relevant physical processes, and ii) the development of more accurate, economical procedures for solving the governing equations.

In connection with inlet tidal motions, a new and efficient procedure was developed for computing periodic flow in deep, narrow inlets. The method is based on a harmonic analysis in which accurate representations of the nonlinear terms in the equations of motion are developed by successive approximation. At each iteration, the modal coefficients satisfy a system of first-order equations and boundary conditions which are combined in such a way as to promote algorithmic efficiency. The method appears to be both accurate and economical--typical computation times for deep inlets may be less than 10% of that required by conventional time-stepping procedures.

The recommendations for deep inlet tidal dynamics follow somewhat the same lines as those for the time-averaged circulation mode. More specifically, the one-dimensional, time-dependent model developed under this grant should be extended to two dimensions, thereby allowing representation of cross-channel flows where they are important (in fact, that extension is now in progress under sponsorship of the National Science Foundation). Beyond that, the formulation should be modified to allow for effects of stratification, and the method should be checked by applying it to a deep inlet region with a fairly complicated shoreline.

3) HYDRAULIC MODEL STUDIES

The Puget Sound hydraulic model in the Department of Oceanography at the University of Washington was used to define detailed surface circulation patterns throughout Puget Sound at various stages of the tide. Four sets of photographs of tidal mosaics were produced which give a qualitative description of the surface flow configuration at different stages of the tide throughout the entire Sound. In addition, a continuous dye injection study was performed

with the hydraulic model to define deep water movement and pollutant pathways at depth for selected locations in Puget Sound near Seattle (at the METRO sewage outfall site at West Point and in Elliott Bay), as well as at seven dredge disposal sites indicated by the Region X office. An edited set of 16 mm films of these studies was given to the Environmental Protection Agency, along with an informal report describing the work and our interpretation of the results. The film and reports may be obtained by contacting the project officer.

The techniques developed for the tidal current study have been satisfactory in most respects, and the results are adequate for a description of the gross surface features of the tidal circulation. Additional work along this line should be aimed at improving the sampling scheme and, in particular, it would be desirable to undertake some combination of the following for certain locations in the Sound: increase the sampling frequency, improve the spatial resolution, and shorten the averaging (exposure) times.

3) BIOLOGICAL MODELING

The overall purpose of the biological modeling effort was to examine relationships between seasonal algal growth, nutrient availability, and gravitational convection in the central basin of Puget Sound, using one of the aforementioned hydrodynamic models and a numerical model of phytoplankton growth. By means of "numerical experiments", the relative importance of various factors influencing algal standing stock in the central basin was assessed, particularly for the spring and summer months. A detailed report was prepared describing not only this aspect of the work, but also earlier phases, including field measurements of central basin topography and biological activity over several years' time.

It was concluded that phytoplankton growth in the central basin of Puget Sound is governed by a combination of factors, including vertical advection and turbulence, modulation of underwater light intensity by self-shading and inorganic particulates, sinking of algal cells, and occasional rapid horizontal advection of algae from the central basin by sustained winds. The high primary productivity of the Sound is due to intensive upward transport of nitrate by the gravitational convection mechanism. It would appear that during the spring and summer months the quantity and quality of freshwater runoff in the central

basin is such as to maintain moderately intense gravitational convection without producing an excessively turbid, brackish, surface zone. On occasions of sustained winds, standing stock is limited by relatively short residence time determined by horizontal advection. Episodic nitrate depletion of a few days' duration, together with a succession of cloudy days, will discourage vigorous growth and will cause blooms to decline in intensity. The effects of grazing by zooplankton and cellular sinking appear to be of secondary importance in the central basin. Because of the rather rare occurrence of nutrient limitation during the spring and the light limitation that prevails during the fall and winter months, nutrient addition from sewage treatement plants is not likely to change the level of primary production in the main channel significantly; perhaps species composition is altered, but no direct evidence of it is at hand. It is also concluded that the functions and parameters traditionally employed to describe phytoplankton metabolism are marginally adequate for use in a short-time scale numerical model of primary production. Our present ability to describe quantitatively the response of phytoplankton to changing environmental stimuli is too limited to permit the construction of predictive models of algal growth which are both reliable and generally applicable to all deep inlets.

The clear indication from our work here is that additional studies of fundamental biological processes at the base of the marine food web are essential. Improved quantitative descriptions are needed of mechanisms by which cells take up, store, and utilize nutrients, mechanisms of light adaptation, changes in cellular chemical composition, and the respiration function. Zooplankton grazing, bacterial activity, and algal response to deleterious substances are also topics which require further study. So far as the central basin of Puget Sound is concerned, it is recommended that biweekly field sampling of the sort described in Section 5 be maintained to monitor water quality on a long term basis. Occasional intensive surveys during different seasons would be a useful supplement to such a sampling program and would also provide additional insight into connections between biological mechanisms and various environmental processes in Puget Sound.

SECTION 5

CIRCULATION MODELING

The deep inlets along the coastline of the Northeastern Pacific Ocean are typically a few kilometers in width, tens of kilometers long, and hundreds of meters deep, except possibly for sills located near the mouth. It is also typical that fluid motions in these deep inlets are dominated by two circulation modes: quasi-steady state or time-averaged gravitational convection and periodic tidal motion. In the course of this project, three different mathematical procedures have been used to represent the flow pattern and density distribution associated with the gravitational convection mode; each method is outlined in some detail in the next three subsections. In the last subsection, a new procedure is described for computing periodic tidal flow in deep, narrow inlets.

5.1 STEADY GRAVITATIONAL CONVECTION: TWO-LAYER ANALYSIS

In an inlet with appreciable freshwater runoff, time-averaged horizontal currents characteristically form a two-zone circulation pattern variously referred to as "gravitational convection" or "estuarine circulation". The freshwater input to the inlet produces a longitudinal pressure gradient which drives a brackish near-surface zone persistently seaward, while at greater depth, a dense saline zone moves landward. The water in this deeper zone is derived largely from sea water external to the inlet, although it may be freshened somewhat by brackish water from above due to turbulent mixing between the zones. This is particularly the case if there is a sill near the inlet mouth. It may also happen that a relatively shallow sill partially isolates deep basin water from oceanic water external to the inlet, thereby creating a third zone of relatively stagnant water in the inlet interior. In this report, gravitational convection is treated on the basis of a two-layer representation (with mixing), although the procedures outlined here could be modified to deal explicitly with a three-layer formulation in which an intermediate transition zone is included.

The discussion is restricted to time-averaged conditions with a view to providing a quantitative description of the quasi-steady state component of

inlet flow. Consider a straight, deep, narrow inlet of length L. The flow parameters and topographic variables are referred to a Cartesian system where the coordinate origin is taken as the mean free surface level near the inlet mouth. The x-coordinate denotes horizontal distance along the inlet axis, measured from the mouth and reckoned positive landward, and the z-axis is directed vertically upward, as shown in Fig. 1.

Fluid motion and density distribution in the inlet is described in terms of a two-layer model, which is derived along lines similar to those used in analysing single-layer channel flow. Subscripts 1 and 2 are used to denote variables in the lower and upper zones, respectively. It is assumed that the fresh water in the inlet is introduced exclusively into the upper layer with zero horizontal velocity (except at $x = L$) at a cumulative volumetric rate given by $R(x)$; (thus, $R(x)$ denotes the total influx between x and L). Because of the typically small depth of the near-surface layer, its breadth $b(x)$ may be taken as constant over its depth. Let d_2 be an appropriate fixed reference depth, such as the zonal thickness at the inlet head, and denote by h_1, h_2 the displacements of the lower and upper surfaces, respectively (Fig. 1). The cross-sectional area of the near-surface layer, denoted by $A_2(x)$, can be written as

$$A_2(x) = b(x)\,[d_2 + h_2(x) - h_1(x)].$$

Next, suppose that the deep layer has cross-sectional area $A(x)$ when the fluid is at rest; the breadth of its top surface will be $b(x)$. The actual cross-section of the deep layer can then be represented as

$$A_1(x) = A(x) + b(x) + b(x)h_1(x).$$

It will be convenient subsequently to refer to a maximum depth $d_1(x)$ of the deep layer when the fluid is at rest. Finally, the horizontal velocities of the deep and near-surface layers will be denoted by $u_1(x)$ and $u_2(x)$, respectively; each is positive when directed landwards. Equations expressing incompressibility (or conservation of volume) and conservation of mass and horizontal momentum in each layer can now be written down.

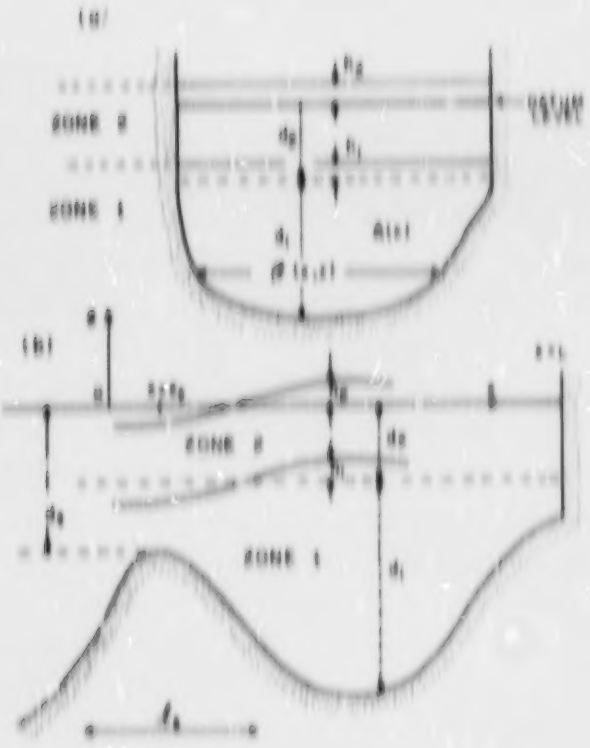

Fig. 1. Sketch of an inlet cross-section (a) and longitudinal section (b), depicting the two major flow zones and illustrating geometrical quantities. The horizontal scale is compressed.

Fig. 2. Sketch of an inlet longitudinal section, illustrating zonal fluid sections used to derive equations of conservation of volume, mass, and horizontal momentum.

In so doing, it is necessary to allow for (upward) convection motion and for turbulent mixing between the layers. In models where flow parameters are continuous functions of depth, vertical transport is described by vertical flow velocities and turbulent fluxes, the latter involving eddy coefficients of viscosity and diffusion. Since turbulent exchange mechanisms in estuarine flow are not at all well understood, the eddy coefficients are usually assigned values or functional forms which are adjusted until calculated flow and hydrographic patterns are similar to those observed in practice. In layered models of coastal plain and salt wedge estuaries, the approach has not been much different; the traditional procedure is to assign adjustable values to friction coefficients at a zonal interface until some correspondence is achieved between computation and observation. In the present work, convective and turbulent transfer between the layers is represented by two interzonal exchange flux rates denoted by F_u and F_d. The symbol F_u represents the upward volume rate of flow of fluid from the deep layer to the near-surface layer per square meter of interfacial area. Likewise, F_d denotes the downward volumetric flux rate from the upper to the lower layer.

Equations expressing incompressibility or volume conservation for each layer are derived from considerations of volume flow rates in and out of sectional "slices" of thickness Δx, illustrated in Fig. 2. For the deep and near-surface layers respectively, one obtains

$$(u_1 A_1)_x = b(F_d - F_u) \tag{1}$$

and

$$(u_2 A_2)_x = b(F_u - F_d) - R_x, \tag{2}$$

where the subscript x denotes differentiation with respect to x. Similarly the equations expressing conservation of mass in the lower and upper layers are

$$(\rho_1 u_1 A_1)_x = b(\rho_2 F_d - \rho_1 F_u) \tag{3}$$

and $$(\rho_2 u_2 A_2)_x = b(\rho_1 F_u + \rho_2 F_d) + \rho_0 H_x \qquad (4)$$

where ρ_2 denotes the mass density of fresh water. In writing down Eqs. (3) and (4), it has been assumed that horizontal diffusion is negligible compared with advective transport. This is a common assumption in deep inlet studies and is validated by the findings of certain oceanographic field studies of fjord waters (e.g., McAlister et al. 1959; Dyer 1973). On the other hand, it may not be justified in the vicinity of a long shallow sill where tidally induced longitudinal dispersion of mass can become competitive with advection.

To derive the momentum equations, we use the fact that the net force on each slice of fluid, in Fig. 2, must equal the net rate of efflux of momentum from that slice. Consider first the lower slice. The net force on it is made up of a pressure imbalance across its two faces, the pressure force on the sides due to changes in breadth, the horizontal component of the pressure force acting on the interface, and the frictional stress $\tau_f(x)$ acting on the wetted perimeter C_w:

$$-\left[\int_{-[d_2+d_1(x)]}^{-d_2+h_1(x)} p\, B(x,z)\, dz\right]_x + \int_{-[d_2+d_1(x)]}^{-d_2+h_1(x)} p\, B_x\, dz + g\,\rho_2\, b(d_2+h_2-h_1)(h_1)_x + \tau_f C_w$$

$$= (\rho_1 u_1^2 A_1)_x + b(\rho_1 u_1 F_u - \rho_2 g F_d)$$

where p is the pressure, g the acceleration of gravity, and $B(x,z)$ the breadth of the lower layer at vertical position z. The usual convention of shallow water theory is adopted to the effect that p results from hydrostatic forces only, so that

$$p = g\left[\rho_2(d_2+h_2-h_1) + \rho_1(-d_2+h_1-z)\right]$$

In carrying out the differentiation indicated for the first term of the momentum conservation equation above, there is no contribution from the x-dependence of the lower limit, since $B(x, -[d_2+d_1]) = 0$. Furthermore, there is no contribution from this term if the channel has a flat bottom since, in that case, the momentum equation contains an additional term of equal

magnitude and opposite sign. The final result can be written as

$$u_1(u_1)_x = -g\left(\frac{A_1 + A_2 - A}{b}\right)_x - \frac{\tau_i}{\rho_1}\left(\frac{\rho_2 A_2}{b}\right)_x + g\,\frac{(\rho_1)_x}{\rho_1 A_1}\left[\left[(1-\gamma)d_2 - \frac{1}{2}\gamma d_1\right]A - \frac{A_1^2 - A^2}{2b}\right]$$

$$+ \frac{\rho_2}{\rho_1}\frac{bF_x}{A_1}(u_2 - u_1) + \frac{\tau_s C_w}{\rho_1 A_1}\,, \tag{5}$$

where γ is defined by the relation

$$\gamma(-d_2 - \tfrac{1}{2}d_1)A = \int_{-d_2}^{\gamma d_2} z\rho(x,z)\,dz.$$

Clearly, in the case of a rectangular channel, $\gamma = \frac{1}{2}$. A similar line of argument leads to the equation of horizontal momentum applicable to the near-surface layer:

$$u_2(u_2)_x = -g\left(\frac{A_1 + A_2 - A}{b}\right)_x - \frac{1}{2}g\,\frac{(\rho_2)_x}{\rho_2}\,\frac{A_2}{b} + \frac{\rho_1}{\rho_2}\,\frac{bF_x}{A_2}(u_1 - u_2)$$

$$+ \frac{\tau_w b}{\rho_2 A_2} + v_0 u_2\,\frac{R_x}{\rho_2 A_2}\,, \tag{6}$$

where $\tau_w(x)$ is the stress exerted on the upper surface by wind.

Equations (1) - (6) can be regarded as a system of equations for the six unknown dependent variables ρ_1, ρ_2, A_1, A_2, u_1, and u_2. Two integrals can be obtained immediately by adding Eqs. (1) and (2), and Eqs. (3) and (4), respectively:

$$u_1A_1 + u_2A_2 = -R \tag{7}$$

and

$$\rho_1u_1A_1 + \rho_2u_2A_2 = -v_0R\,. \tag{8}$$

These two equations will be used subsequently to eliminate a pair of dependent variables from the system.

All that remains is to specify appropriate boundary conditions. In situations often encountered in practice, the mass density of oceanic water seaward of the inlet mouth is presumed known. In fact, $\rho_1(0)$ is ordinarily the only dependent variable that can be specified at $x = 0$. At the head of the inlet, we take the horizontal velocity in the lower layer to be zero, i.e., $u_1(L) = 0$. Suppose now that a river flows into the head of the inlet, delivering fresh water (of mass density ρ_0) at the volume rate $R(L)$. If d_2 is taken to be

the effective depth of the freshwater zone at $x = L$, where the channel breadth is $b(L)$, then both h_f and h_s can be set equal to zero at $x = L$. Then, since $\rho_s(L) = \rho_0$, it is consistent with Eqs. (7) and (8) to take $u_s(L) = R(L)/b(L)d_s$. The boundary value problem statement is now complete since six conditions have been imposed.

According to the foregoing specification, all but one of the dependent variables are assigned values at the inlet head. Most standard integration methods that might be used to solve the system of six differential equations assume that starting values of all variables are given at the same point. In practice, one could begin the calculations with a provisional value of $\rho_f(L)$ estimated from data and adjust it iteratively until $\rho_f(0)$ is approximately equal to the prescribed value seaward of the inlet mouth.

Since not every inlet possesses a simple, well-defined headwater region, it may be convenient to start the calculation at some distance downstream of the landward terminus. For example, suppose that near the landward end $(x = L)$, fresh water originates in streams that feed a number of small subsidiary embayments where wind mixing of fresh and salt water takes place. In this situation, the total freshwater influx near $x = L$ is still $R(L)$, but the mass density $\rho_s(L)$ must be that appropriate to the brackish water contributed by the embayments. If the depth d_s is now the depth of the brackish zone, h_f and h_s are again set equal to zero. However, the velocity u_f is no longer zero at $x = L$, since continuity implies movement of some saline water into the embayments. The specification of both u_f and u_s follows from Eqs. (7) and (8) after assignment of values to ρ_f and ρ_s and $x = L$. As above, the estimate of $\rho_f(L)$ could be regarded as provisional and could be adjusted until agreement with a prescribed value of $\rho_f(0)$ is achieved.

In applying the model to a particular inlet, it would be desirable to follow a definite procedure for estimating F_u and F_d. There is more than one course of action open at this stage and the choice that is made will depend upon the special circumstances of the problem. For example, on the basis of hydrographic information and other considerations, one might choose to assume that specific transport or exchange mechanisms are dominant and assign appropriate functional dependence to F_u and F_d when such dependence is believed known or can be guessed at (from laboratory experience, for instance).

However, when the main objective is to simulate representative flow in a particular inlet, an attractive alternative is to establish the density distributions by measurements and to express F_u and F_d in terms of the densities and unknown dependent variables by the procedure described below.

Consider a deep, narrow inlet for which the cumulative freshwater input is known and where estimates of the mass densities ρ_I and ρ_E are available from field data. Define auxiliary functions $\phi_I(z)$ and $\phi_E(z)$ by

$$\phi_I = \frac{\rho_I - \rho_0}{\rho_I - \rho_E} \cdot \frac{z}{D} \tag{9}$$

and

$$\phi_E = \frac{\rho_E - \rho_0}{\rho_I - \rho_E} \cdot \frac{z}{D} \tag{10}$$

Since ρ_I and ρ_E are prescribed, the functions ϕ_I and ϕ_E are known, and can be used together with Eqs. (7) and (8) to express the layer cross-sections A_I and A_E in terms of the unknown velocities u_I and u_E:

$$A_I = b\phi_E u_I^{-1} \tag{11}$$

and

$$A_E = -b\phi_I u_E^{-1} \tag{12}$$

These expressions can be used to help eliminate A_I and A_E from Eqs. (5) and (6). Next, it is shown that the factors bF_d/A_I and bF_u/A_E can also be expressed in terms of known (or estimable) functions and the unknown velocities. Thus, Eqs. (1) and (2) may be used in Eqs. (3) and (4) to yield

$$u_I(\rho_I)_x = -\frac{bF_d}{A_I}(\rho_I - \rho_E)$$

and

$$u_E(\rho_E)_x = \frac{bF_u}{A_E}(\rho_I - \rho_E) + (\rho_E - \rho_0)\frac{R_E}{A_E}$$

From these equations, together with Eqs. (9) and (10), it can be shown that

$$F_d = -A_I\phi_E \tag{13}$$

and

$$F_{II} = -\delta_{II}\phi_I \tag{14}$$

where

$$\delta_I = \frac{(v_I)_B}{v_I - v_{II}} \tag{15}$$

and

$$\delta_{II} = \frac{(v_{II})_B}{v_I - v_{II}} + \frac{v_B - v_B}{v_I - v_{II}} \cdot \frac{R_B}{P\phi_I} \tag{16}$$

Since the two auxiliary quantities δ_I and δ_{II} are known, and A_I and A_{II} are given in terms of u_I and u_{II} by Eqs. (11) and (12), the factors F_I and F_{II} are F_I/A_I and F_{II}/A_{II} given in terms of the unknown velocities. It is now clear that the original system of six equations can be reduced to two equations of the form

$$a_{II}(u_I)_B + a_{IB}(u_{II})_B = b_I \tag{17}$$

and

$$a_{BI}(u_I)_B + a_{BB}(u_{II})_B = b_{II} \tag{18}$$

where

$$a_{II} = u_I - \sigma\phi_{II}u_I^{-B}, \qquad a_{IB} = \sigma\frac{v_{II}}{v_I}\phi_I u_{II}^{-B},$$

$$a_{BI} = -\sigma\phi_{II}u_I^{-B}, \qquad a_{BB} = u_{II} + \sigma\phi_I u_{II}^{-B}, \tag{19}$$

and where

$$b_I = -\sigma(\phi_{II})_B u_I^{-1} + \sigma\frac{v_{II}}{v_I}(\phi_I)_B u_{II}^{-1} + \sigma\left(\frac{\phi}{h}\right)_v + \sigma\frac{(v_{II})_B}{v_I}\phi_I u_{II}^{-1}$$

$$+\sigma\frac{(v_I)_B}{v_I} \cdot \frac{u_I}{\phi_{II}}\left[\left((1-\gamma)d_{II} - \frac{1}{2}\gamma d_I\right) \cdot \frac{A}{B} - \frac{1}{2}\left(\frac{\phi_{II}^B}{u_I^B} - \frac{A^B}{h^B}\right)\right]$$

$$-\frac{v_{II}}{v_I}\phi_I u_I(u_{II} - u_I) + \gamma_f\frac{C_M}{B}\frac{u_I}{v_I\phi_{II}}, \tag{20}$$

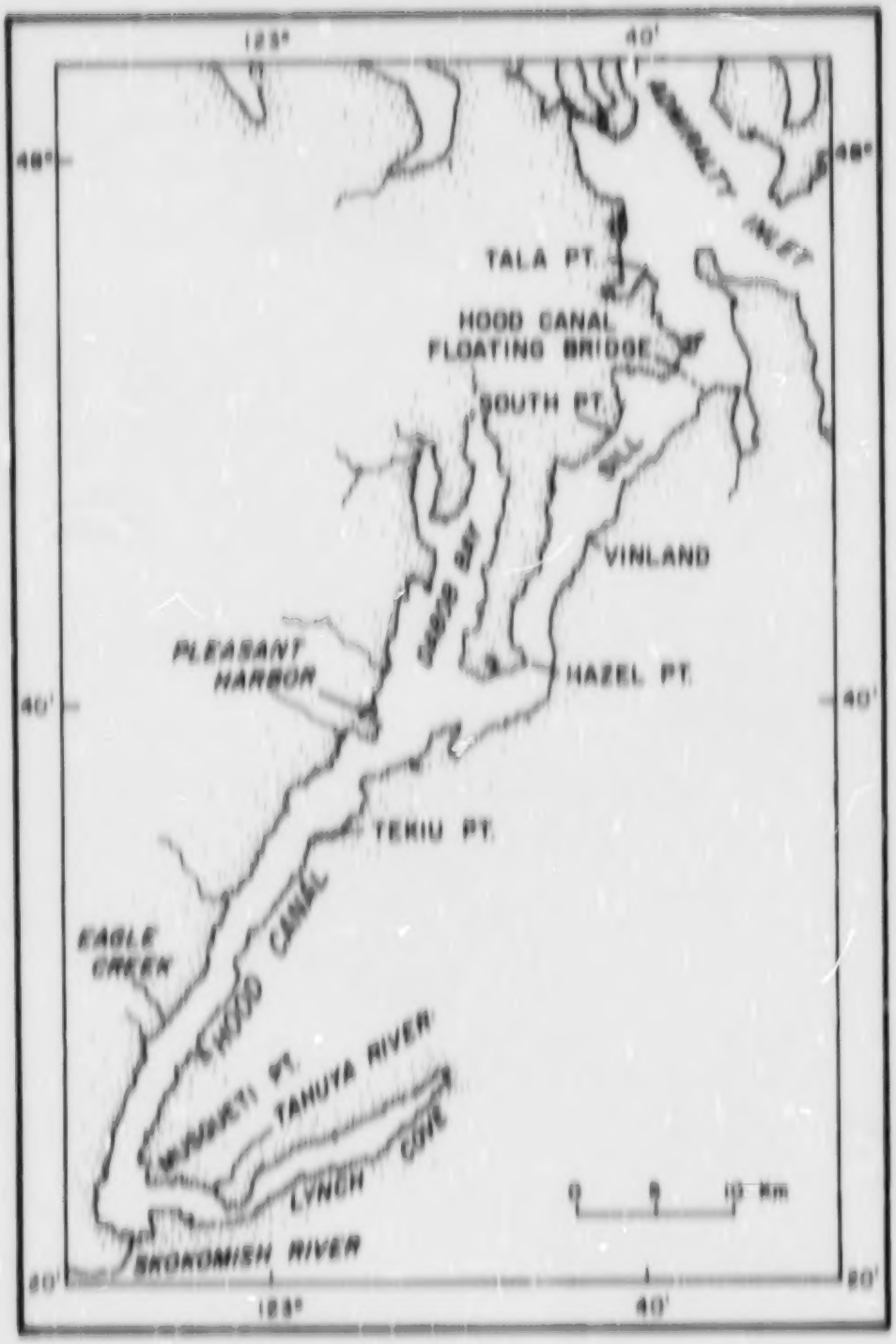

Fig. 3. Map of Hood Canal, Washington.

and $$b_\beta = -g(\phi_\beta)_x u_1^{n+1} + g(\phi_1)_x u_\beta^{n+1} + g\left(\frac{\phi}{D}\right)_x + \frac{1}{\rho_\beta g} \frac{(\rho_\beta)_x}{\rho_\beta} \phi_1 u_\beta^{n+1}$$

$$+ \frac{\rho_1}{\rho_\beta} A_\beta u_\beta (u_1 - u_\beta) - \left(\tau_\omega + \rho_o \frac{R_\beta}{D} u_\beta\right) \frac{u_\beta}{\rho_\beta \phi_1} \qquad (21)$$

The system (17) and (18) is readily solved for $(u_1)_x$ and $(u_\beta)_x$, and the resulting equations can be integrated efficiently by the fourth-order Runge-Kutta method.

For the purpose of illustration, the procedure just outlined has been applied to Hood Canal, Washington. Hood Canal is a deep inlet nearly 100 km long and 1 to 3 km wide, on the western side of the Puget Sound system (see Fig. 3). Puget Sound as a whole communicates with the Pacific Ocean by way of the Strait of Juan de Fuca to the north. The principal entrance to the Sound is through Admiralty Inlet, a relatively shallow channel with a 50 m deep sill, between the Olympic Peninsula and Whidbey Island. Hood Canal opens into Admiralty Inlet near Tala Point, about 15 km south of the sill. As can be seen from the bathymetric profile in Fig. 4, Hood Canal itself has a 50 m deep entrance sill near Vinland, about 20 km south of the inlet mouth near Tala Point. Landward of the Vinland sill, the basin deepens to 160 m in the central segment. The Hood Canal basin is characteristically steep-sided, with shelves which are either very narrow or non-existent. Near the northern end is Dabob Bay, a small, deep subsidiary inlet. At the southern terminus of the basin is a relatively shallow appendage, Lynch Cove, whose axis forms an acute angle with the main axis of Hood Canal.

Fresh water in Hood Canal is derived from land drainage, rainfall, and river runoff. A large fraction of the land area adjacent to the Canal is drained by five main rivers that are distributed along the inlet axis as shown in Fig. 3. Freshwater input to the inlet is greatest during the early winter months when rainfall is most intense. The seasonal river discharge cycle exhibits a peak at that time and a secondary peak in the late spring due to snow melt in the mountains within the watersheds on the western side of the Canal.

In considering this particular application of the model, we recognize that, since Hood Canal is a relatively low runoff inlet, it is seldom strongly

stratified (see Fig. 4) and, therefore, a two-layer representation is perhaps only marginally appropriate. Despite its shortcomings, however, the results of the two-layer analysis have been shown to be reasonably consistent with alternative approaches (see Winter and Pearson, 1976). The two-layer representation is most likely to be justified following the later summer replacement of deep basin water and during the autumn period of heavy rainfall. Figure 6 shows surface layer and deep zone salinities typical of this season at nine different locations along the basin axis. (Salinity is defined here as grams of salt per kilogram of sea water.) The data shown in the Figure are averages of salinity measurements acquired in nine cruises conducted during the months of October and November from 1951 through 1963.

Autumnal conditions in Hood Canal were simulated in the following way: first, it can be deduced from a study by Friebertshauser and Duxbury (1972) that, during the months of October and November, the average total volumetric freshwater inflow rate to Hood Canal is approximately 145 m^3/sec. Next, it is assumed that the distribution of cumulative runoff along the inlet is proportional to cumulative drainage area, which can be reconstructed from the watershed areas shown in Fig. 8. This reconstruction gives the data points plotted in Fig. 7. The overall variation of $R(x)$ is represented approximately by the function

$$R(x) = 145, \qquad \text{for } 0 \le x \le 20 \text{ km}$$

$$= 145 \exp\left[-\left(\frac{x - 20}{50}\right)^2\right], \qquad \text{for } x > 20 \text{ km}, \tag{33}$$

shown as a dashed line in Fig. 7. A plot of the approximate representation of Hood Canal bathymetry is given in Fig. 5. The breadth of the main channel was taken to be constant and equal to 2 km.

Next, in order to specify the auxiliary functions ϕ_1, ϕ_2, δ_1, and δ_2 in Eqs. (9), (10), (15), and (16), respectively, it is necessary to generate approximate representations of ρ_1 and ρ_2 from salinity measurements acquired during the late autumn months. Inspection of profiles of salinity at several locations along the axis of Hood Canal suggests that the nominal depth of the near-surface layer is roughly 15 m over the greater part of the inlet. Salinity data from nine stations in all were averaged over two depth intervals, 0 to 15 m and 15 m to the bottom, with the results shown

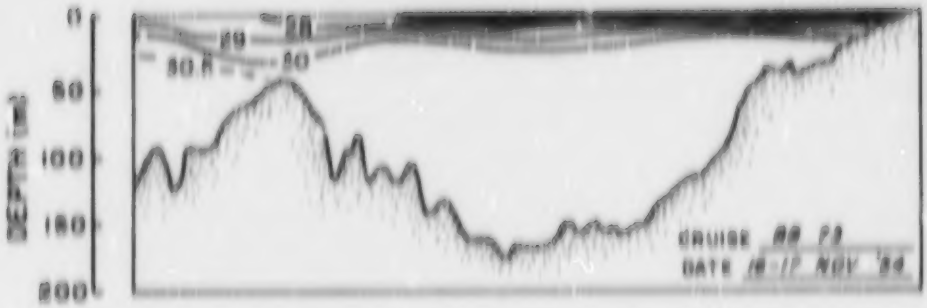

Fig. 4. Bottom profile of Hood Canal, Washington, and salinity isopleth configuration in mid-November 1954.

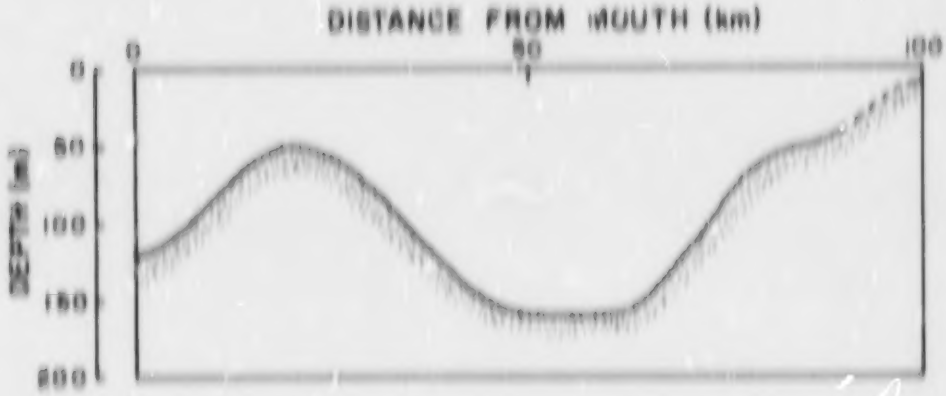

Fig. 5. Idealization of Hood Canal bottom profile used in model calculation.

in Fig. 6. A consideration of the graphs in Fig. 6 indicates that, as a first approximation, we may neglect the refluxing effect near the Vinland sill and take ρ_f to be constant throughout the deep zone. If we assume a linear equation of state, then ρ_f takes the value

$$\rho_f = 1000 + 0.77 S_f \approx 1023.4 \text{ kg/m}^3$$

where S denotes salinity and where the coefficient of S is appropriate to the autumnal water temperature range in Hood Canal. The longitudinal variation of salinity S_s in the near-surface layer can be approximated by a Gaussian function of x, thereby providing a functional representation of ρ_s for substitution into the equations for the auxiliary functions.

In the model equations, the wind stress on the upper surface was taken to be zero on the average. The boundary stress τ_f was assumed to be related to the horizontal speed u_f in accordance with the Chezy-type relation

$$\tau_f = -\delta\, u_f\, |u_f|\, D^{-1/6} \qquad (23)$$

in newtons/m^2, if u_f is in m/sec, and D in m. (One newton = 10^5 dynes.) This last relation is one frequently used in the literature for frictional stress; the coefficient δ represents a mean value of typical reported coefficients. Actually, in most deep inlet applications, boundary stress will not make an important contribution to the overall horizontal momentum balance.

In order to specify the boundary conditions, recourse is made to field data. Consideration of representative salinity profiles for the region, the runoff distribution in Fig. 7, and the topographical relation between Hood Canal and Lynch Cove, suggests the desirability of starting the calculation near the confluence of Lynch Cove and the southern end of the main basin. According to the earlier discussion of boundary conditions, the nominal terminus of the inlet can be taken to be at $x = L = 90$ km. $R(L)$ will then be the river discharge at 90 km as calculated from Eq. (26) (near the Skokomish and Tahuya Rivers). Salinity profiles indicate that an appropriate value for d_s is roughly 15 m. Next, the value of s_s at $x = L$ can be obtained from the approximate representation $S_s(x)$ mentioned above. Then, since ρ_f is equal to a constant (evaluated earlier), sufficient information is available to determine the starting values of horizontal velocities u_f and u_s consistent with

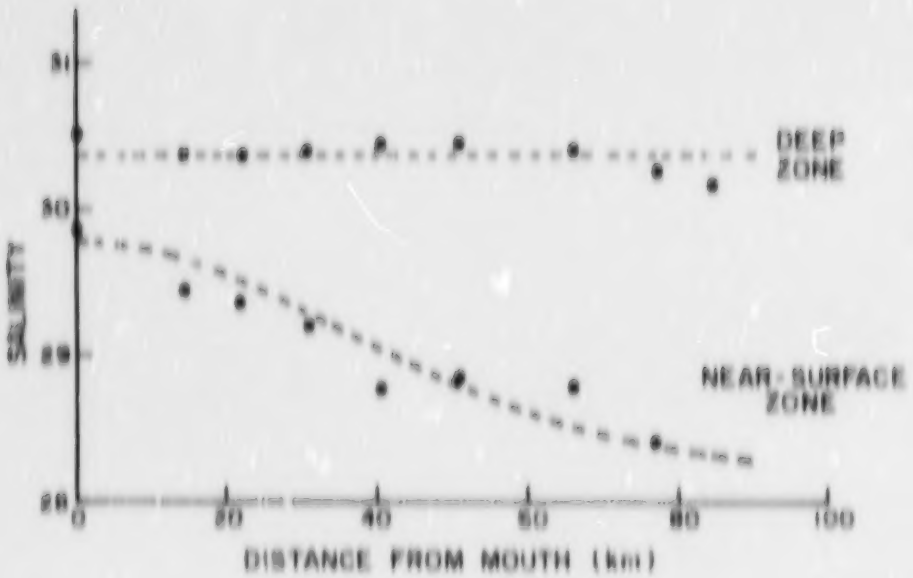

Fig. 6. Axial variation of deep and near-surface zone salinity in Hood Canal during October and November.

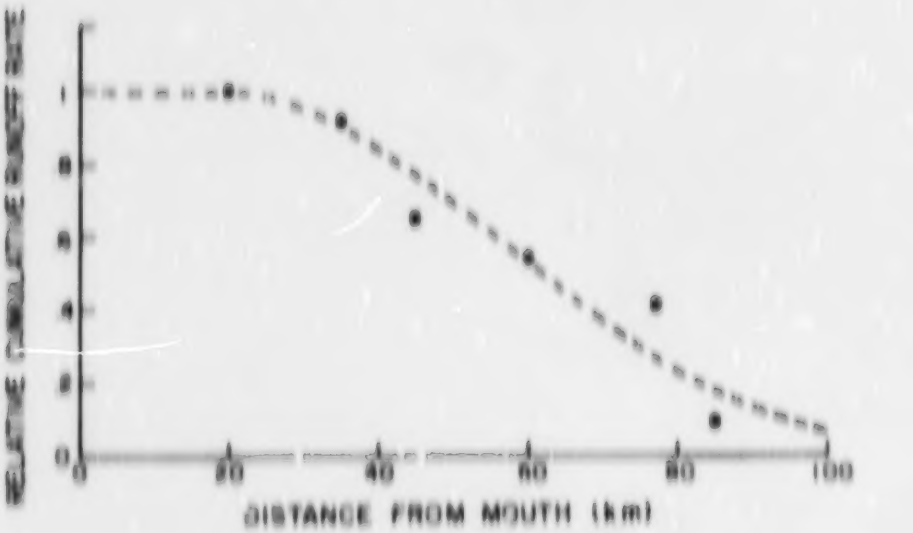

Fig. 7. Relative cumulative runoff rate in Hood Canal.

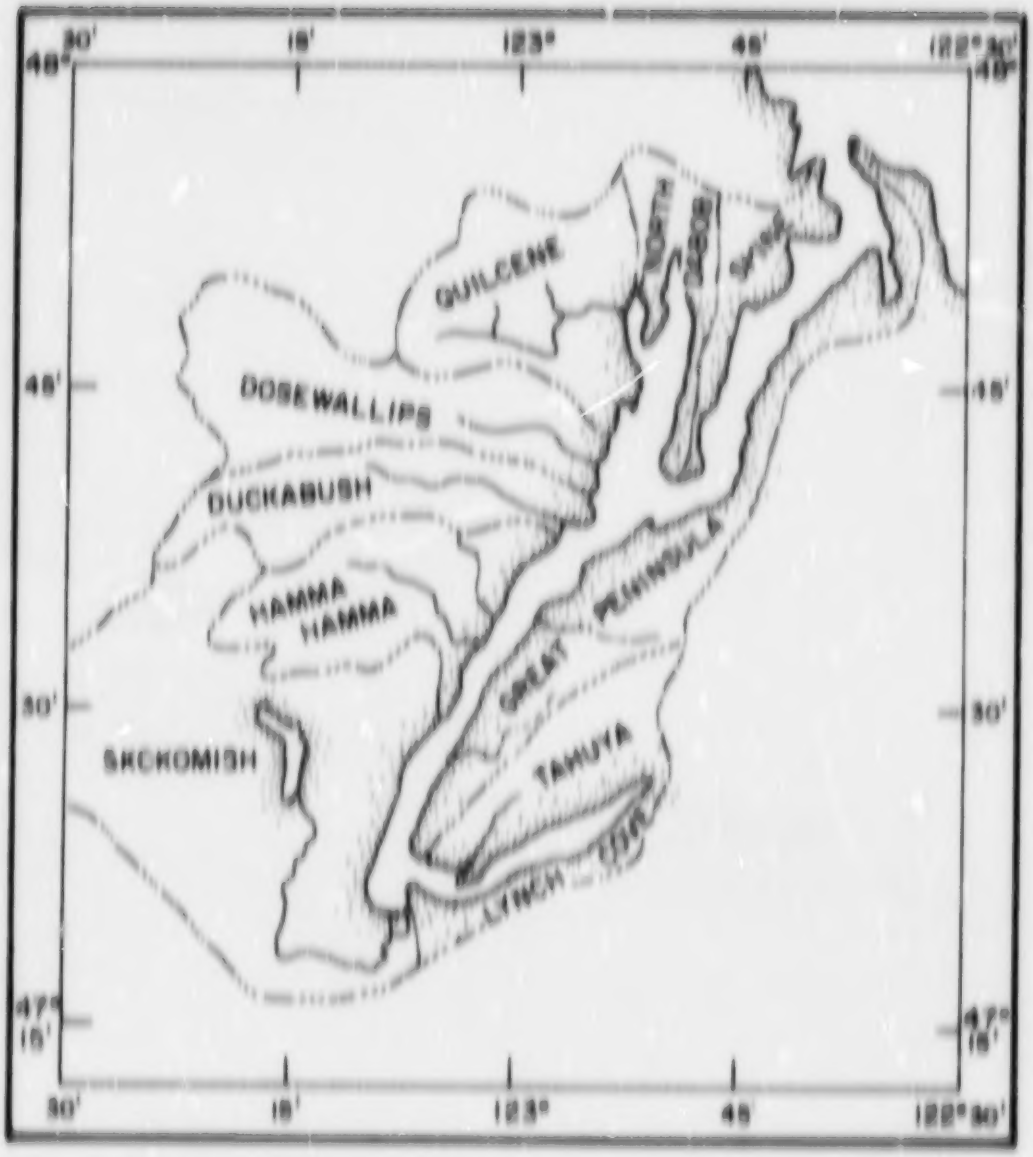

Fig. 8. Principal drainage basins of Hood Canal.

Eqs. (7) and (8). The system of differential equations for u_j and u_β was then solved by a fourth-order Runge Kutta procedure, for the domain $0 \leq x \leq 90$ km, subject to the boundary conditions above. Calculated horizontal speeds and the zonal interface depth are given in Fig. 9 along with a graph of the depth longitudinal variation of F_u. Current speeds and the calculated zone depths seaward of the Vinland sill are in rough agreement with preliminary current meter results for that region (Applied Physics Laboratory, University of Washington, unpublished). However, since no tidal-average current measurements are available for other locations in the inlet, no further comparisons can be made. Hence, an assertion that the model has been validated on the basis of the existing data would be an overstatement of the case. On the other hand, what has been done is to develop an approximate, self-consistent representation of horizontal currents and density distribution believed to be characteristic of Hood Canal during the late autumn months. The calculated results are in reasonable accord with the limited amount of field data available for comparison purposes.

It should be clear from the foregoing illustration of the method that the model can be applied with relative ease to an inlet with fairly complicated bathymetry and distributed runoff. A model of this type could be conveniently used in connection with pollution studies. Thus, if estimates were required of soluble contaminant distributions in a deep inlet, the model can easily be supplemented with equations of the type (3) and (4) describing pollutant mass distributions in the near-surface and lower zones, with appropriate terms appended to describe the source and (possibly) the loss of contaminant throughout the inlet.

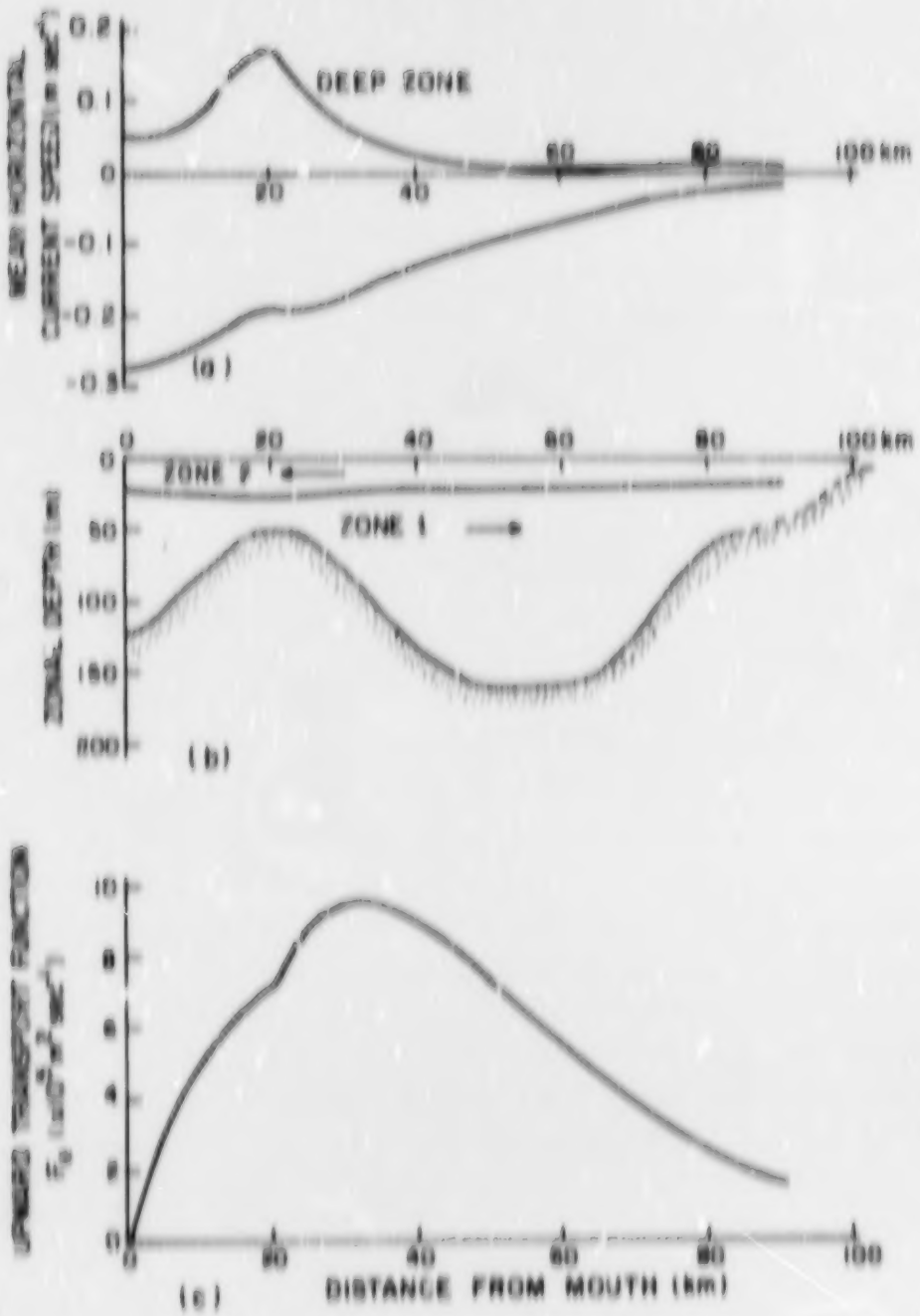

Fig. 9. Calculated axial variations of mean horizontal current speed (a), zonal depth (b), and upward transport function P_u (c) in Hood Canal for October and November.

3.2 STEADY GRAVITATIONAL CONVECTION: SIMILARITY ANALYSIS

Although the two-layer model is relatively easy to apply, it suffers from several disadvantages: for example, 1) mass density and horizontal velocities are represented as discontinuous functions of depth, 2) vertical transport by advection and turbulent mixing is not represented in a straightforward way, and 3) in contrast with the implications of a two-layer representation, it is observed that the vertical scale associated with the horizontal current often exceeds that of the mass distribution. On the other hand, it is very difficult to generate continuum descriptions of gravitational convection in deep inlets. Two attempts to solve the problem by the use of similarity analysis have been reported [Rattray (1967), Winter (1973)]. The latter work was performed under the sponsorship of the Environmental Protection Agency and is summarized herein.

As mentioned at the beginning of this section, the flow in deep inlets with appreciable freshwater input is characterized by a reversal in the direction of horizontal current at depth. When most of the fresh water comes from river discharge near the head of the inlet, and when winds are light-to-moderate, the circulation tends to a two-layer system in which the uppermost layer moves persistently seaward above a landward-moving deeper layer of saltier water. Up-inlet winds retard the outflow and may sometimes exert sufficient stress to reverse the direction of the surface current, causing outflow to occur in an intermediate zone at several meters depth below the surface (Pickard and Rodgers, 1959). Three-zone flow may also occur locally in fjord segments when the longitudinal distribution of freshwater runoff increases fast enough in the seaward direction to produce a landward-directed pressure head near the surface. However, the present discussion is restricted to deep inlets with runoff distributions which, in the absence of wind stress, produce a seaward-directed mean surface current. Also, consideration is limited to inlet segments which are narrow and sufficiently straight that cross-channel pressure and velocity differences are small and Coriolis forces can be neglected. Under these conditions, field accelerations in the upper regions of the flow may contribute to the overall horizontal momentum balance as well as the horizontal pressure gradient and the vertical gradient of the turbulent stress. As mentioned in the previous subsection, field studies in Silver Bay, Alaska,

performed by McAlister et al. (1959) suggest that horizontal diffusion plays a negligible role in the upstream transport of salt in fjords.

The steady-state equations are obtained by time-averaging the equations of motion over a tidal cycle. In addition, the governing equations are laterally averaged over the channel width. In this analysis, the spatial dependence of all variables will be referred to a Cartesian coordinate system whose origin is at mean sea level, located near the head of the section under consideration. The positive x^*-axis extends horizontally in the seaward direction and the z^*-axis is taken to be positive downward. Variables with asterisk superscripts are quantities with dimensions; variables without asterisk are nondimensional.)

The usual assumption is made that the time-average of the turbulent stress can be represented by the product of the horizontal velocity shear and a suitably defined vertical eddy coefficient of viscosity N_B^*. It is further assumed that the turbulent flux of salt can be adequately represented by the product of a vertical eddy coefficient of diffusion K_B^* and the vertical gradient of the mean salinity S^*.

It is convenient to express the governing equations and the final results in terms of nondimensional variables. In the case of deep, stratified inlets, an appropriate scale in the vertical direction is the thickness of the brackish surface zone within which most of the fresh-water runoff is transported to the sea. Field studies of the fjord-type inlets (see, for example, Tully, 1949; Pickard, 1961, 1971) suggest that the depth z_0^* of the brackish surface zone can remain within the decameter range over inlet segments which are tens of kilometers in length. A measure of the total time-mean rate of outflow is given by the ratio of the cumulative volumetric runoff rate R_0^* and the fractional excursion σ_0 from great depths to the surface:

$$\sigma_0 = \frac{S_\infty^* - S_B^*}{S_\infty^*} \tag{24}$$

where S_∞^* is the salinity at great depth and S_B^* is the surface salinity. (The subscript zero is used here and in the sequel to denote appropriate reference station values in the inlet segment under consideration.) Since the outflow takes place in a zone whose thickness is of the order of z_0^*, by

definition, an appropriate measure of the horizontal velocity is given by the characteristic speed u_0^* in the upper zone

$$u_0^* = A_0^* b_0^* s_0^* a_c, \tag{25}$$

where b_0^* is the reference channel width. It is appropriate to measure longitudinal distance in units which reflect the fact that the horizontal scale a_0^* is determined by the balance between mixing and advective salt transport. The turbulent transport of salt is described by a suitably defined vertical eddy diffusivity of the order of K_0^*, say, near the surface. Estimates of K_0^* in fjord-type circulations place this parameter in the range of 0.1 to 10 cm^2/sec (Trites, 1955; Cade, 1968). When K_0^* can be assigned a value from field measurements or from estimates in comparable inlets, the vertical velocity can be measured in units of

$$w_0^* = u_0^* s_0^* / a_0^* \tag{26}$$

where the horizontal scale is given by

$$a_0^* = u_0^* s_0^{*2} / K_0^* . \tag{27}$$

The analysis is facilitated by replacing the salinity S^* with a nondimensional salinity defect $F(x,z)$ defined by the relation

$$\frac{S_0^*(x,z)}{S_0^*} = 1 - s_0 F(x,z) \tag{28}$$

where s_0 is the dilution factor given by Eqn. (2). With this definition, the salinity defect at the reference station is equal to unity at the surface and approaches zero at great depth. It is also assumed that the vertical eddy diffusivity K_0^* is a constant fraction δ of the kinematic eddy viscosity N_0^*/ρ_0^*, where ρ_0^* is a reference density; values of δ inferred from field studies lie in the range of 1 to 10^{-2}, with the smaller values corresponding to stronger stratification (Trites, 1955). The nondimensional vertical eddy diffusivity is denoted by K and is, in general, a function of the nondimensional space coordinates, x and z.

The foregoing developments can be used to show that the nondimensional steady-state velocity field (u,w) and the salinity defect F are determined by a

system similar to the one given by Mattray (1967). In the derivation of the equations, Coriolis accelerations are neglected, and the hydrostatic and Boussinesq approximations are used:

Incompressibility:

$$(bu)_x + (bw)_z = 0 \tag{29}$$

Equation of Salt:

$$(buF)_x + (bwF)_z = (bKF_x)_x \tag{30}$$

Equation of Horizontal Momentum:

$$\Delta t(uu_x + \bar{w}u_z) = (Ku_x)_x - \frac{Rf}{g^*}\zeta_x + Rf\int_{-\zeta}^{\eta} F_x(x,z)dz \tag{31}$$

where $\zeta(x)$ is the free surface height. The overall flux Richardson number Rf is defined by

$$Rf = \Delta\, g^*\varepsilon\, \sigma_0 z_0^4/u_0^{*2},$$

where g^* is gravitational acceleration and ε is the differential density parameter from the approximate equation of state

$$\frac{\rho^*}{\rho_0^*} = 1 + \varepsilon\frac{T^*}{T_m^*}.$$

Upon taking the x-derivative of Eq. (31), one obtains an alternative form in which the free surface height does not appear:

$$\Delta t(uu_x + \bar{w}u_z)_x = (Ku_x)_{xx} + Rf\, F_x \tag{32}$$

A stream function can be defined in the usual manner, and is conveniently measured in units of z_0^* so that

$$bu = -\psi_z \quad \text{and} \quad bw = \psi_x.$$

The system is to be solved in the domain $z \geq 0$ and $|x| \leq L^*/z_0^*$, say. The boundary conditions at the surface require specification of the wind stress τ_w^*

$$-Ku_z = \left(\frac{\Delta u_0^*}{K_0^* u_0^* \rho_0^* z_0^*}\right)\tau_w^* = \tau_w \quad \text{at} \quad z = 0$$

and the integral mass flux

$$\psi(x,0) = R(x) \tag{33}$$

At great depths, the velocity components, the vertical salt flux, and the salinity defect approach zero. The problem statement is supplemented by the requirement that the integral of the horizontal salt flux over each section of the inlet is zero. This leads to integral salt flux constraint whose non-dimensional form is

$$\int_0^\infty huF\,dz = R(x),$$

where the integral mass flux has been equated to the cumulative runoff.

Now, consider an inlet segment in which the channel breadth $b(x)$ and the cumulative runoff rate $R(x)$ can be represented approximately as powers of exponential functions

$$R(x) = \exp(\alpha x) \quad \text{and} \quad b(x) = \exp(\beta x).$$

Introduce new independent variables by

$$\xi = \exp(x) \quad \text{and} \quad \eta = z \exp(\lambda x).$$

Then, the expressions for the equations of motion and the integral salt flux constraint suggest a search for solutions of the form

$$\psi = \xi^{\mu} f(\eta) \quad \text{and} \quad F = \xi^{\nu} g(\eta)$$

provided the eddy viscosity can be expressed as

$$K = \xi^{\pi} D(\eta).$$

A similarity solution is appropriate when the exponents μ, ν, and λ are such as to permit cancellation of all factors involving ξ in the governing equations. According to Eq. (33) for the integral mass flux, similarity would require the longitudinal variations of cumulative runoff and surface velocity to be the same. Since this is not always characteristic of inlet flow, it is convenient to replace Eq. (33) with an approximate condition. According to Hattray (1967), when the freshwater runoff is a small fraction of the total circulation,

$$\psi(x,0) \neq 0, \tag{34}$$

With the approximate condition (34), it can be shown that a similarity solution can be sought when the several exponents of ξ satisfy the relations

$$\mu = \frac{1}{6}\alpha + \frac{2}{6}\beta + \frac{1}{2}\kappa$$

$$\nu = \frac{3}{6}(\alpha - \beta) - \frac{1}{2}\kappa$$

$$\lambda = \frac{1}{6}(\alpha - \beta) - \frac{1}{2}\kappa \qquad (35)$$

and the nondimensional wind stress is given by

$$\tau_w = \left(\frac{a_0^4}{\rho_0 \overline{w'u'}_0}\right)\tau_w^* = \tau_0\, \xi^{\frac{1}{6}(\alpha-\beta)+\kappa}$$

where the constant τ_0 is calculated from the prescribed wind stress at a central station in the inlet.

In order to proceed, a further assumption is made concerning the spatial dependence of the eddy viscosity coefficient. The depth variation of turbulent stress inferred in the aforementioned Silver Bay study (McAlister *et al.*, 1959), considered together with the observed horizontal velocity shear, implies that the eddy viscosity coefficient decreases with depth through the halocline and then may increase somewhat at greater depth. The same trends have been reported in a study of Oslo Fjord by Gade (1968) who observed a minimum in K_B^4 (~0.05 cm^2/sec) in the lower part of the brackish phase. The coefficient K_B^4 was observed to increase nearer the surface where it attained values of 1 to 10 cm^2/sec. Both Gade (1968) and Trites (1955) report a tendency of K^4 in fjords to increase in the seaward direction. Near the surface the eddy viscosity may depend in some way upon the wind stress (Kullenberg, 1971) or upon the character of the flow and density distribution through the local Richardson number; however, dependence is not determined at this writing. Since the present study is concerned only with the upper layers, a simple exponential dependence on depth is assumed

$$D = \exp(-\eta).$$

When the exponent conditions expressed by Eq. (35) are satisfied, the governing equations reduce to a definite integral and two coupled nonlinear ordinary differential equations for f and g:

$$\int_0^\infty f'g\,d\eta = -1,$$

$$A\left[\mu ff''' - (\mu + 2\lambda - \beta\beta)f'f'\right] = (\mu f'')'' - Rf(\nu g + \lambda\nu g')$$

and

$$\nu f g' - \nu f' g = (\beta g')',$$

where the prime indicates differentiation with respect to η. The boundary conditions at the surface are

$$f(0) = 0, \qquad g(0) = 1$$

and the stress condition gives

$$f''(0) = \tau_0 .$$

The conditions at great depth require

$$f(\infty) = f'(\infty) = 0,$$

In the paper by Winter (1973), an approximate solution for the stream-function and the salinity defect is developed from series representations of f and g, valid in the upper zone:

$$f = e^{-\eta} \sum_0^\infty a_m \eta^m$$

and

$$g = e^{-\beta\eta} \sum_0^\infty d_m \eta^m .$$

The reader is referred to Winter (1973) for details of the derivation.

For the purpose of illustration, the aforementioned approximate similarity solution was applied to segments of Hood Canal and the central basin of Puget Sound, Washington. Since the main purpose was to demonstrate the method of analysis, the overall flux Richardson number was set equal to one-half, a value appropriate to conditions of moderate to high stability (Bowden and Gilligan, 1971). Trites (1955) used current and density data in several British Columbia inlets to estimate Richardson numbers and found large variations of Ri with depth. However, average values were generally in the range 10 to 50. This finding suggested the assignment of a value of 25 to the overall Richardson number $Ri = Rf/A$. This implies a value for A of 1/50, which

is consistent with estimates in comparably stratified waters. Trites (1955) also observed that the width of inlet flow was usually smaller than the geographical width of the estuary. Hence, in the calculations, values of b_0^* were estimated by reducing the geographical widths by 25 percent. The variations of channel width in Hood Canal were judged to be unimportant ($\beta = 0$). In the central basin of Puget Sound, the bathymetric charts suggest a slight general widening in the seaward direction. The longitudinal variations in cumulative runoff for the central segment of Hood Canal and the Puget Sound central basin were inferred from the distribution of drainage basin areas as done in the previous subsection. Values of α and β appropriate to each inlet segment and a segment of Knight Inlet, British Columbia, are given in the paper by Winter (1973).

Data from various field studies were adopted for comparisons with the computations [estimated values of the parameters b_0^*, R_0^*, and K_0^* appropriate to the midsegment station and time period of each field study are also presented by Winter (1973)]. The vertical and horizontal length scales can be calculated from these parameters when the appropriate dilution factors σ_0 are specified. The down-inlet variations in eddy viscosity were inferred from observed longitudinal variations of surface salinity in Hood Canal. In the case of Puget Sound, longitudinal variation of surface salinity over the central basin segment is usually rather slight: about 0.5 parts per thousand over 40 km, on the average. This value can be used to infer κ when runoff is low to moderate, but leads to small, negative values of κ when river discharge is high. Therefore, κ was set equal to zero in the latter instance.

Figure 10 shows a comparison of the calculated isohaline distribution in Hood Canal with that observed during the month of April 1953, as reported by Barlow (1958). Figure 11 shows salinity measurements acquired during two three-day periods at a mid-channel station in the central basin of Puget Sound in the spring of 1966. The periods shown correspond to runoff episodes of high and moderate intensity, respectively. The solid lines in the figure show the salinity distributions derived from the present theory. Theoretical horizontal and vertical velocity profiles for the high runoff case are also shown in the figure. Unfortunately, simultaneous measurements of salinity

Fig. 11. Comparison of measured and calculated isohaline configuration in a longitudinal section of Suez Canal; the data were acquired at the stations shown in the map.

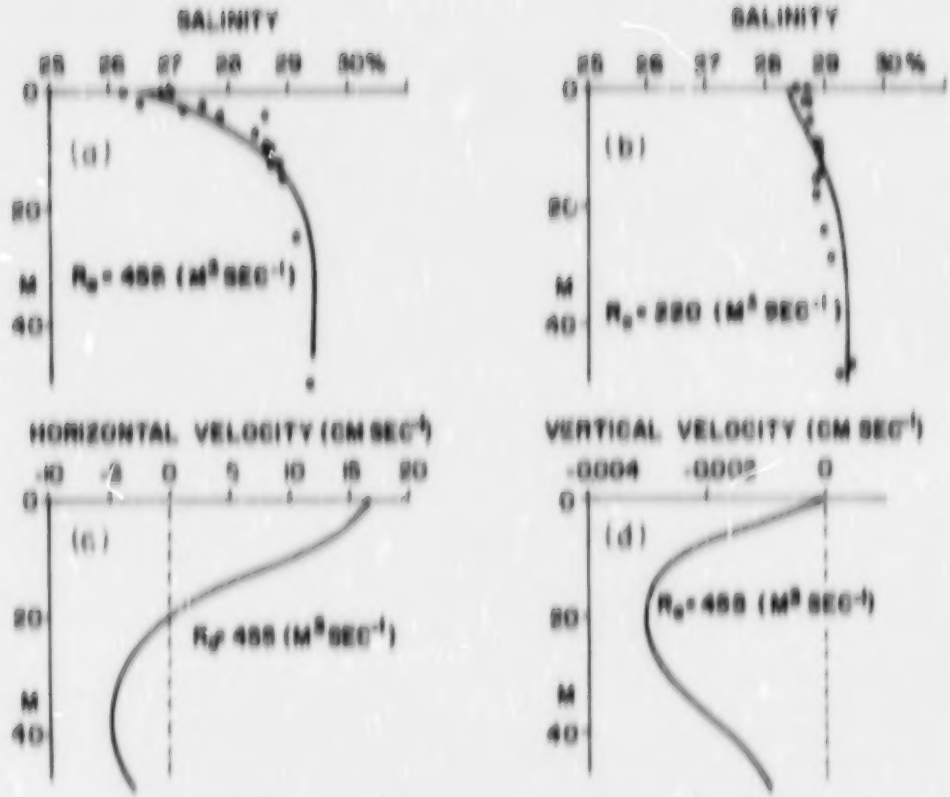

Fig. 11. Comparison of calculated depth profiles of salinity and salinity measurements acquired in May 1966 at a mid-channel station in the central basin of Puget Sound for (a) a relatively high runoff rate: R_o = 455 m^3 sec^{-1} and (b) a moderate runoff rate: R_o = 220 m^3 sec^{-1}. Velocity profiles for the high runoff period are also shown: (c) horizontal component; (d) vertical component.

and horizontal velocity are unavailable for this particular station and time of the year. However, rough comparisons can be made with current data acquired at other central basin stations by Paquette and Barnes (1951) and, more recently, by Cannon and Laird (1972) during the month of February 1971. In both sets of measurements, the time-mean surface outflow is of the same order as that which was calculated, but the measured depth of no mean motion exceeds the calculated depth by 10 to 15 meters. This latter discrepancy is probably due to effects associated with an underwater promontory near the sites of the measurements.

In the two cases examined here, different sets of parameter values might possibly bring theory and observation into even better agreement. However, the comparisons in the figures are good enough to indicate that similarity analyses may be useful when approximate analytic descriptions are needed of the principal features of flow and density distribution in deep, stratified inlets.

3.3 STEADY GRAVITATIONAL CONVECTION: METHOD OF WEIGHTED RESIDUALS

Despite some limited success achieved with similarity techniques, the procedure suffers from at least two important disadvantages: 1) restrictive interrelationships are imposed on variables which are normally unrelated, such as the longitudinal variation of width, runoff, and wind stress,and 2) it is necessary to solve coupled, nonlinear ordinary differential equations. The series solutions obtained by Rattray (1967) and Winter (1973) are valid only in the near-surface zone and are first approximations, at best. An attempt was initiated in this project to circumvent the aforementioned disadvantages by using weighted residual techniques. Since the effort is still in progress at the time of this writing, only the highlights of the approach will be outlined here.

The starting point of the analysis is the set of equations describing steady-state gravitational convection in inlets, as given by Eqs.(29), (30), and (31). The dependent variables are the salinity defect $F(x,z)$ and the horizontal and vertical velocity components $u(x,z)$ and $w(x,z)$, respectively. These variables are referred to a Cartesian coordinate system whose origin is near the free surface, and where x is positive seaward along the inlet axis and z is positive downward. As before, the governing equations are solved subject to the appropriate boundary conditions at the free surface expressing continuity of volume, horizontal stress, and salt flux. In the present work, the flux boundary conditions were applied at $z = 0$, although the free surface height $\zeta(x)$ was retained in the Equation of Horizontal Momentum. Again, when the primary interest is in the near-surface circulation, one may neglect the effects of bottom topography and friction by assuming the inlet to be infinitely deep, as is done in the similarity analysis:

$$F,\ u,\ u_z,\ w \to 0 \text{ as } z \to \infty\ . \tag{36}$$

Of course, the assumption of infinite depth is not essential to the application of the method. Finally, starting conditions are imposed at an appropriate inlet station x.

It is convenient to employ an alternative form of the Horizontal Momentum Equation when the inlet is infinitely deep. In view of the conditions expressed by (36), one may take the horizontal gradient associated with the

free surface slope to be balanced at great depth by that associated with the mass density distribution, so that

$$\zeta_x = \varepsilon\sigma_0 \int_{-\zeta}^{\infty} F_x(x,s)\, ds, \tag{37}$$

where σ_0 is a reference value of the fractional salinity excursion from great depth to the surface. It follows from Eq. (31) that

$$\delta(uu_x + wu_s) = (Ku_s)_s - Rf \int_s^{\infty} F_x\, ds. \tag{38}$$

The boundary value problem just described can be solved by the weighted residual method as outlined briefly below. First, the horizontal velocity $u(x,s)$ and the salinity defect $F(x,s)$ were approximated by trial function expansions of the following forms:

$$u(x,s) = \sum_{j=1}^{N} u_j(s) f_j(x)$$

$$F(x,s) = g(x)\phi(s)$$

where u_j and ϕ are prescribed functions of s, chosen to satisfy the boundary conditions at depth. The functions f_j and g are undetermined coefficients in the expansions and depend only upon x. An expression for the vertical velocity $w(x,s)$ is obtained at once by integrating the incompressibility condition:

$$w(x,s) = v_j(s)\left(f_j' + b^{-1}b' f_j\right)$$

where $b(x)$ is the inlet breadth, the prime denotes differentiation with respect to x, and where

$$v_j(s) = \int_s^{\infty} u_j(s)\, ds.$$

Next, the above representations of u, w, and F are substituted into Eqs. (30) and (38) (Conservation of Salt and Horizontal Momentum, respectively) to give equations of the general form

$$\sum_{j=1}^{N} \{f'_j(x)A_j(f_k,g)(x,z)\} + g(\nabla\cdot)B(f_k,g)(x,z) + \sum_{j=1}^{N} D_j(f_k,g)(x,z) = Ro_k(x,z)$$

If ϕ, u_j, f_j and g satisfied the equations of motion exactly, the right-hand side of this last expression would be equal to zero. Since this is not the case, the combination on the left is equal to some "residual function" which has been denoted by $Ro_k(x,z)$. The essence of the method of weighted residuals is to determine the functions f_j and g in such a way that the residual Ro is small in some sense. Possible procedures for doing this are the Method of Moments, Galerkin's Method, Collocation, etc.

In summary, it is necessary to determine $N+1$ unknown functions; specifically, N functions f_j and the function g. The unknown free surface height $\zeta(x)$ can be subsequently obtained from Eq. (37). For this determination, we require $N+1$ equations. Boundary conditions and the integral salt flux constraint provide three independent equations. The remaining $N-2$ equations are obtained by one of the procedures mentioned above. The important observation to be made is this: although one is dealing with coupled, nonlinear, first-order differential equations, the equations are nevertheless linear in the z- derivatives and can be solved accurately and efficiently by, say, the Runge-Kutta method; the solution of nonlinear algebraic equations for derivative values is not necessary. Moreover, it can be shown, after some algebraic manipulation, that this statement also holds true if turbulent mixing coefficients are functions of the local Richardson number. This feature makes the method of weighted residuals particularly attractive as a mathematical technique for solving deep-inlet flow problems. Figure 12 presents the results of a sample calculation using the method of weighted residuals, with inlet parameters appropriate to Knight Inlet, British Columbia. A Galerkin procedure was used to establish the equations governing the unknown functions, as described above. Coefficients of eddy viscosity N and diffusion K were assumed to decay exponentially with depth $N, K \sim \exp(-z/z_0)$; also $u_j = \exp(-z/z_0)(z/z_0)^{j-1}$ and $\phi = \exp(-z^2/z_0^2)$ where z_0 is the

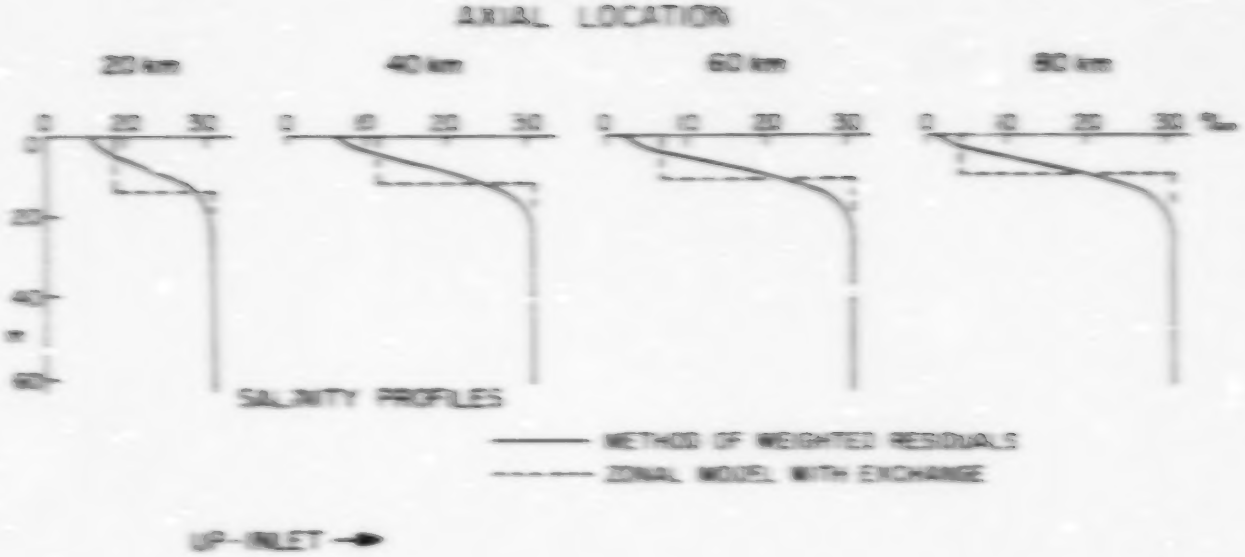

Fig. 12. Comparisons of salinity profiles throughout Knight Inlet, B.C., as calculated by the weighted residual method and by the two-layer analysis. Axial location is distance upstream of the inner sill.

vertical scale of the gravitational convection zone (Winter, 1973). Starting conditions were chosen to simulate conditions near the seaward end of the deep inner basin in Knight Inlet. Computed results over a 60 km segment of the inner basin are shown in Fig. 12; these results compare favorably with field observations, as reported by Pickard and Rodgers (1959).

3.4 PERIODIC TIDAL MOTION IN NARROW INLETS

Consider a deep, narrow inlet in which the tidal motion may be analysed in terms of one-dimensional shallow water theory. The relevant equations express conservation of volume, mass, and horizontal momentum. Because of the periodic nature of tidal phenomena, a harmonic analysis of the equations of motion seems particularly attractive. However, the presence of nonlinear terms introduces complications, so that some kind of approximation is necessary. In this phase of the modeling work, a new approach was developed to harmonic analysis of tidal motion based on an iterative numerical expansion of the nonlinear terms into frequency components. The inlet geometry may be fairly arbitrary, so long as cross-channel motions are relatively unimportant (an extension to two-dimensional time dependent tidal flow is in progress).

The coordinate system as used in this analysis is illustrated in Fig. 13. The distance x is measured upstream from the south, and the upstream direction is taken as positive. The velocity $u(x,t)$ (where t is time) is assumed constant over each cross-section; the height of the water surface above reference level is denoted by $h(x,t)$. The cross-sectional estuary is $A(x)$ and we take the effective top breadth as $b(x)$, so that the net cross-sectional area at any value of x and t is given by $(A + bh)$. From shallow water theory, the equations of motion can be written in the form

$$u_t + gh_x + Fu = f_1 \tag{39}$$

$$h_t + b^{-1}(Au)_x = f_2 \tag{40}$$

where g is the acceleration of gravity, and where the quantities f_1 and f_2 represent the effects of friction, wind stress, lateral drainage, and convective acceleration.

F is an appropriately-chosen positive constant, and the term Fu may be thought of as an artificial friction term, introduced for purposes of

Fig. 13. Narrow inlet geometry.

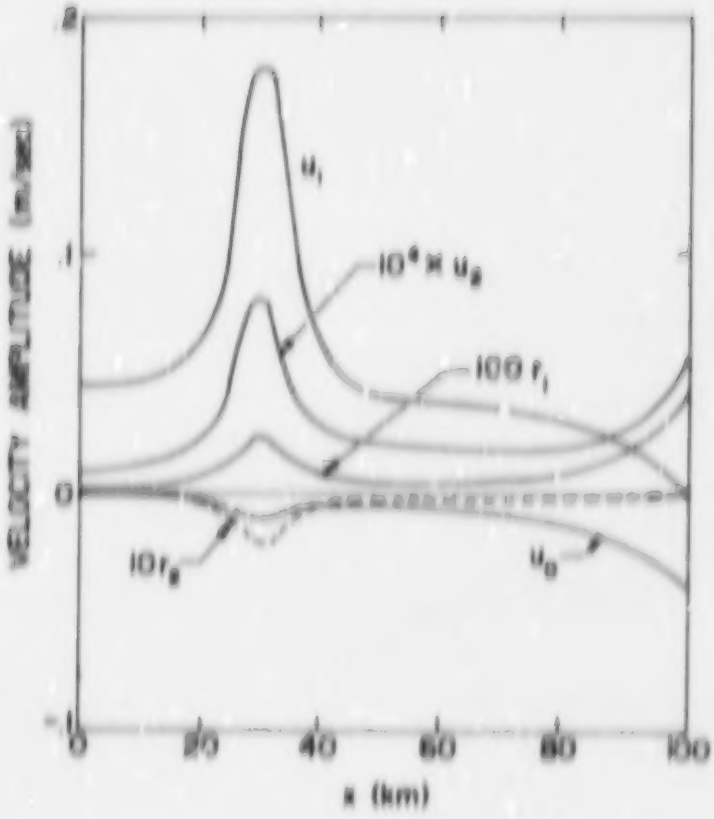

Fig. 14. Axial variation of velocity mode amplitudes for model inlet.

computational stability. The same term is included in f_I, so that the term Fu has no net effect, once iterative convergence is complete.

To illustrate the calculation of f_I and f_{II}, consider a situation in which the estuary density ρ is approximately constant and in which there is no freshwater inflow. Denote the wind stress by τ_w and the frictional stress by τ_f; one then has

$$f_I = Fu - \omega_w + \frac{\tau_w - \tau_f}{\rho(d+h)} + \frac{\tau_f}{\rho H} \tag{41}$$

$$f_{II} = -\frac{1}{b}(bhu)_x \tag{42}$$

where H is the hydraulic radius. As mentioned earlier in Section 3.1, τ_f may be given by an expression that might be of the Chezy-Manning type:

$$\tau_f = -C\frac{u|u|}{H^{1/3}}$$

where C is a constant.

Denote the fundamental period by T and the angular frequency by $\omega = 2\pi/T$. In the case of some estuaries, a particular sequence of tidal patterns may not repeat itself for several weeks. Nevertheless, in a great many applications, it will be adequate to choose T to be some small multiple of the dominant tidal constituent, such as the period of the M_2 tide. (It might be noted that competitive time-stepping methods must address a similar question in that it is necessary to decide how long a time history is to be included in the calculation.) If the first N modes are of primary interest, then $u(x,t)$ and $h(x,t)$ are approximated by

$$u(x,t) = \frac{u_0(x)}{2} + \sum_{n=1}^{N}\left[u_n(x)\cos\omega nt + v_n(x)\sin\omega nt\right] \tag{43}$$

$$h(x,t) = \frac{h_0(x)}{2} + \sum_{n=1}^{N}\left[h_n(x)\cos\omega nt + a_n(x)\sin\omega nt\right] \tag{44}$$

where $u_n(x)$, $v_n(x)$, $h_n(x)$, $a_n(x)$, for $n = 0, 1, 2, \ldots, N$, are x-dependent expansion coefficients. These coefficients are determined by use of Eqs. (39) and (40), together with f_I and f_{II} defined as in Eqs. (41) and (42).

The method used is one of successive approximation, and proceeds as follows. Suppose that at any stage of the iteration approximate values for these expansion coefficients have been determined. Then, by use of Eqs. (43) and (44) each of u and h can be calculated, and can in turn be used to compute f_1 and f_2 (within the current degree of approximation) for any chosen values of x and t. But if one can calculate f_1 and f_2, then these quantities can also be expanded in a Fourier series, via

$$f_1(x,t) = \frac{a_0(x)}{2} + \sum_{n=1}^{N} [a_n(x) \cos n\omega t + b_n(x) \sin n\omega t]$$

$$f_2(x,t) = \frac{\alpha_0(x)}{2} + \sum_{n=1}^{N} [\alpha_n(x) \cos n\omega t + \beta_n(x) \sin n\omega t]$$

For least mean square error, we require, for $n = 0, 1, 2, \ldots, N$,

$$a_n(x) = \frac{2}{T} \int_0^T f_1(x,t) \cos n\omega t \, dt \quad \text{and} \quad b_n(x) = \frac{2}{T} \int_0^T f_1(x,t) \sin n\omega t \, dt$$

with analogous formulas for $\alpha_n(x)$ and $\beta_n(x)$. These coefficients, $a_n(x)$, $b_n(x)$, $\alpha_n(x)$, $\beta_n(x)$ are determined by direct numerical integration (for periodic functions, the trapezoidal rule is optimal) for those values of x which occur as mesh points in the sequel. It is, of course, only necessary to evaluate f_1 and f_2 for those values of t which arise in this numerical integration.

Having now determined $a_n(x)$, $b_n(x)$, $\alpha_n(x)$, $\beta_n(x)$, all terms in Eqs. (39) and (40) are replaced by their Fourier expansions, and terms of the same frequency are equated to obtain a system of coupled first-order differential equations for the unknown variables u_0, h_0, u_n, h_n, v_n, and δ_n. So far as the boundary conditions are concerned, some conditions are given at one end of the inlet, and some at the other end. Thus, at $x = 0$, the tidal fluctuation is imposed, so that each of $h_n(0)$, $\alpha_n(0)$ is known for $n = 0, 1, 2, \ldots, N$. At the upstream limit $x = L$, we take the total flow rate Q as prescribed, where

$$Q = u(L,t)[B(L) + b(L)h(L,t)] \tag{45}$$

Since $h(L,t)$ is unknown, it is necessary to include the determination of $u(L,t)$ as part of the iterative process. At each iteration stage, the

current value of $h(b,t)$ is used to compute a best value for $u(b,t)$, which is again expanded in Fourier terms to give current values for $u_n(b)$, $r_n(b)$, $n = 0, 1, \ldots, N$, and so to provide upstream boundary conditions for the modal equations. For a complete discussion of the modal equations and the method of solution, the reader is referred to a paper by Pearson and Winter (1976). In that paper, it is shown that a particular combination of the first-order modal equations yields second-order equations, which may be discretised so as to result in tridiagonal coefficient matrices, making two-sweep elimination feasible.

The calculation of the modal coefficients is now repeated iteratively until the mesh-point values of the coefficients no longer change significantly. If nonlinearities are weak, one or two such iterations may be adequate; if strong, as many as 15 or more may be required. It is only in the latter case that we need assign to F a value different from zero.

In the paper by Pearson and Winter (1976), the procedure is illustrated by an application to a 100 km segment of a river in communication with the sea. Since nonlinearities were large in that example, the problem posed considerable challenge to the method. An accurate result was obtained (a comparison was made with results from a time-stepping solution) and convergence was complete after 10 iterations (90 seconds on a CDC 6400).

As another example, consider a deep inlet with a sill, where the bathymetry is described by

$$b(x) = 2000 - 0.015x \quad (x \text{ in metres})$$

and

$$A(x) = b(x)(200 - 0.0016x)\left[1 - 0.75 \exp\left[-\left(\frac{x - 10,000}{10,000}\right)^2\right]\right]$$

for $0 \leq x \leq 100,000$ metres. Suppose that all of $h_n(0)$ and $u_n(0)$ are set equal to zero, except that $u_1(0) = 1$; also, set $Q = -315$ m^3/sec. The time profiles of $h(x,t)$ for various values of x are now not too dissimilar to that of $h(0,t)$; only the first two modes are significant. The effect of the sill (at $x = 30,000$) is seen most clearly in a plot of the modal components of $u(x,t)$ as given in Fig. (14). For this problem, only 1 iteration (5 seconds on a CDC 6400) was required; the value of F was set equal to zero.

Finally, it should be pointed out that the method can be applied to situations

in which the inlet is branched. A description of the necessary modifications of the procedure is given by Pearson and Winter (1976).

SECTION 4

HYDRAULIC MODEL STUDIES OF PUGET SOUND

Puget Sound is a system of fjord-type inlets with complicated tidal circulation patterns induced by irregular bathymetry and shoreline. Since its dynamic tidal behavior is so complex, reliable qualitative and quantitative descriptions are often very difficult to obtain by field observations alone without intensive and costly efforts. This suggests that studies of tidal motions with the Puget Sound hydraulic model could provide a valuable guide for efficient design of field studies and/or monitoring activities that may be indicated. Tidal flows are important in Puget Sound because they are comparable with (and in some regions greater than) the mean flow (Cannon and Laird, 1978). In nearly all parts of the Sound, a large fraction of the energy associated with the fluid motion is contained in the tidal mode.

Previous studies have demonstrated that hydraulic model tidal currents, circulation, and water exchange are generally representative of the prototype and will provide a reliable means of investigating gross dynamic characteristics within a relatively short time (Battray and Lincoln, 1955). Before proceeding with a discussion of the model studies, however, a brief description of the model itself is in order.

4.1 MODEL DESCRIPTION AND LIMITATIONS

The "Puget Sound Model" is a small working model of the entire system of inland waterways extending south from the junctions with the Strait of Juan de Fuca and Rosario Strait (see Fig. 15). The model has a horizontal scale of 1:40,000 or 25 mm per m (1.82 in./naut. mile, 1.58 in. per stat. mile) and a vertical scale of 1:1152 or 1 meter = 0.868 mm (1 foot = 0.0087 in.). The model thus has a vertical exaggeration of 35:1. These scales correspond to a time scale of 1:1,178 or 3.056 seconds per hour.

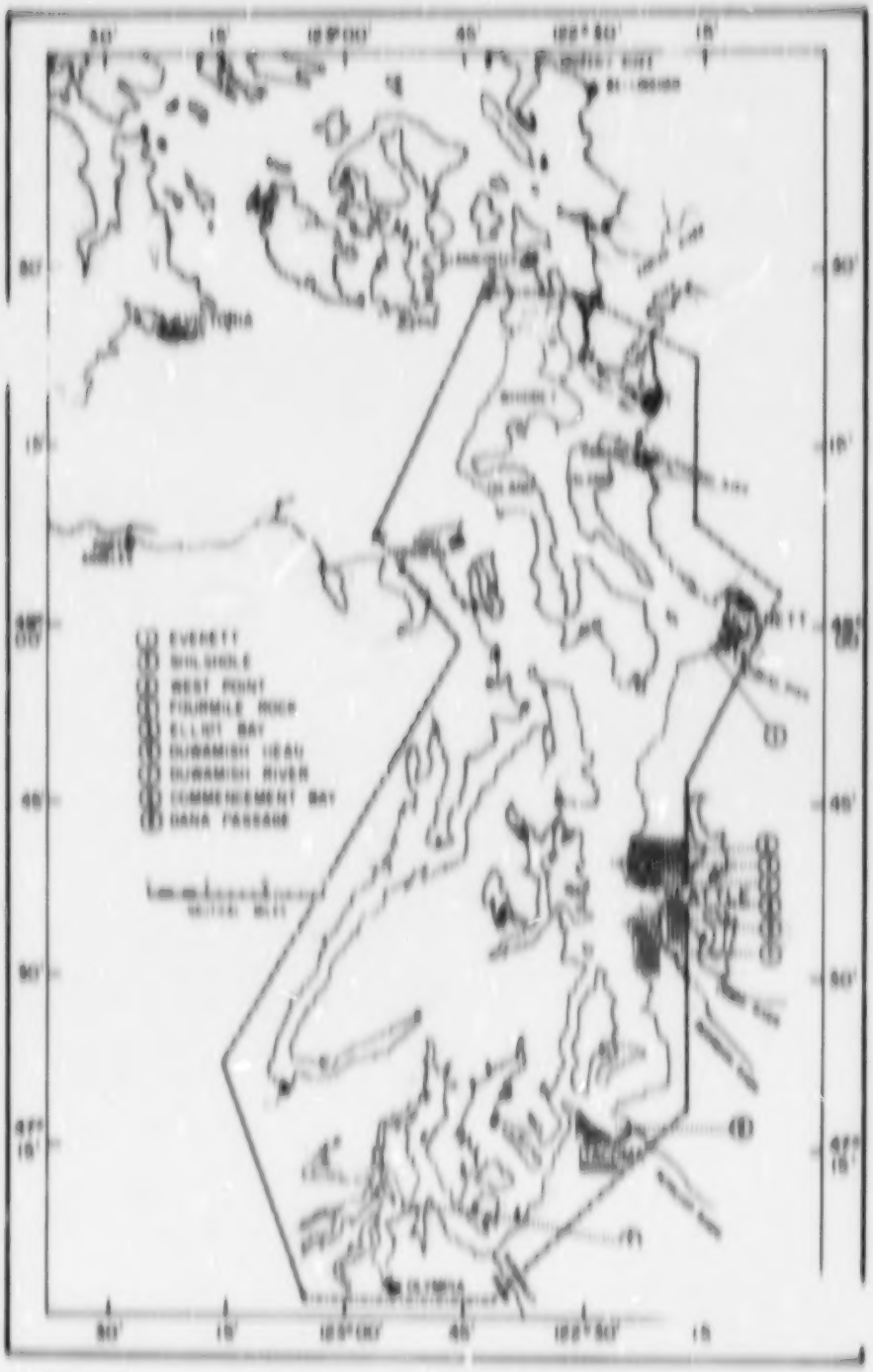

Fig 15. Hydraulic model coverage (outlined by dashed line) and the locations of the dye discharge experiments.

Tides in the model are controlled by a Kelvin-type mechanical tide computer that provides continuous summation of six cosine functions representing the six major tide constituents. This analog computer controls the vertical motion of a plunger which generates the tides by displacement of the appropriate volume of water in the model headbox, which is located in the inner end of the Strait of Juan de Fuca. The tide computer provides the capability of generating model tides for any specific calendar time period which agree with predicted tide heights to within 0.15 scale meters (0.5 scale foot).

The model operates as a stratified system to provide a representation of the natural density gradients within Puget Sound which drive the net circulation. An ocean-tank provides a source of constant salinity water that is recirculated between the ocean tank and the headbox. Fresh water is introduced at appropriate rates at the sites of the eleven major rivers discharging into Puget Sound. River discharge is manually controlled and indicated by individual precision flow meters.

Not all physical phenomena can be adequately scaled in the model, and there are a number of constraints on the interpretations of the results. These limitations are as follows:

1) Wind stress effects cannot be scaled properly, thus model observations are representative of calm wind conditions only. This is perhaps the most important limitation because surface transport and mixing of the water by winds can be significant factors in dispersal processes. In the prototype, winds will induce wave action and exert stresses on the free surface that will modify near-surface flow characteristics.

2) Surface tension cannot be eliminated or even appreciably reduced. This effect distorts representation of flows just at the surface, close to the shoreline, and in very shallow areas.

3) Water viscosity cannot be reduced to scale. This results in a reduction of small-scale turbulence and mixing, and slightly retards flow through small channels at times of strong currents. Various considerations, such as the requirement of representative density gradients, make the use of a lower-viscosity fluid impractical.

A) Because of the vertical exaggeration of 15:1, required for dynamic similitude, horizontal flows are quantitative but vertical motion is only qualitative.

Two types of studies were performed with the hydraulic model in this phase of the project. The first study was an attempt to define tidal current patterns throughout the Sound, and was carried out by photographing the hydraulic model water surface motions as revealed by styrofoam powder.

The second was a model study of dye-stream dispersal characteristics in selected locations throughout the Sound, with special attention given to dredge spoil disposal sites. These studies are described in separate subsections below.

4.2 SURFACE TIDAL CURRENTS IN PUGET SOUND

Eight mosaic photographs of the entire Puget Sound model surface were assembled to indicate the surface current distribution for eight stages of a hypothetical, but representative tide. The direction and magnitude of the flow were indicated in the photographs as white "stream lines", with the length of the line proportional to the speed. Graphs were affixed to each photograph showing the stage of the Seattle tide at the time of the photograph. Copies of the mosaic photographs were provided to the Region X office and the Project Officer of EPA. For the purpose of this report, a hand-drawn replication of a part of the mosaic for one stage of the tide is provided as Fig. 16. A complete set of such surface tidal current patterns is being prepared for publication at the time of this writing under the sponsorship of Washington Sea Grant.

In the present studies, recording was done photographically on 35 mm Plus-X black and white film. To obtain the tidal current flow lines, white or light-colored particles were photographed against a dark background. The dark background was achieved by coloring the water an intense red with Congo Red dye and attaching a green filter (X-1) to the camera. The dye-filter combination resulted in the water photographing as black, giving high contrast with the white floating particles.

Fig. 16. Hand-drawn replication of part of the tidal mosaic for one stage of the tide; direction and magnitude of surface tidal current is indicated by orientation and length of streamline segments.

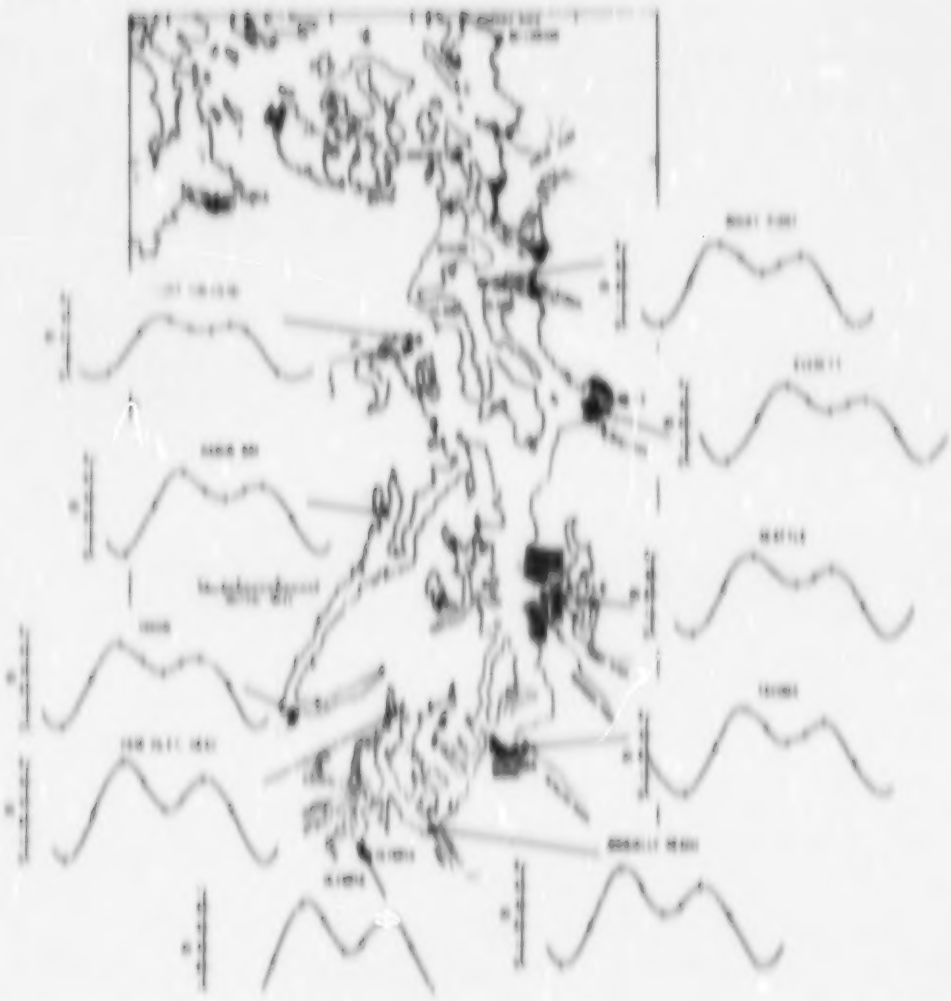

Fig. 17. Map of Puget Sound showing the measured model tides; dots on the tide curves correspond to the time of the eight streamline photographs.

To mark the surface movement, we experimented with aluminum dust, lycopodium powder, pollen, and finely divided styrofoam. Of these materials, the powdered styrofoam appeared to be most suitable for the surface floating particles.

To simplify the experimental procedures, repeating tides with semidiurnal and diurnal frequencies were used in the model. The amplitudes and phases of these two tidal components were computed to produce a representative mixed tide at Seattle. The resulting tide heights, as recorded in the model for Seattle and other locations around Puget Sound, are illustrated in Fig. 17. Photographs of the model were taken vertically from a height of about 2 m above the water level. Because of the limited spatial coverage of the photograph, fourteen separate camera locations were required to cover the entire area of the model. At each location, 2-second time exposures were made (corresponding to 40 minutes of model time) for each of eight stages of the tide. The beginnings of the exposures were chosen to correspond to the times of highs, lows, and maximum slopes of the tide curve at Seattle. These times are shown in Fig. 18. Because tides at other sites within Puget Sound are slightly out of phase with respect to Seattle, the exposure times are not synchronized to local lows, highs, and maximum flows. The choice of repeating tides allowed us to run the model continuously and to take the eight tidal sequence photographs at each of the different locations without restarting the natural tide sequence in the model.

All river outflows were adjusted to model yearly mean discharge rates and were held constant for the duration of the study. The "ocean" salinity was held constant at 16‰; previous experience has indicated that the vertical salinity profile better approximates the prototype when the model "ocean" salinity is maintained at this reduced level.

As mentioned earlier, the photographs showing the streamlines for each of the eight stages of the tide were assembled to produce eight mosaics of the tidal currents in Puget Sound. The original negatives for these photographs are on file at the Department of Oceanography, University of Washington, and enlarged, detailed prints of selected locations and specific tide stages can be supplied at cost. Some of the major flow features which emerged from this study are described below.

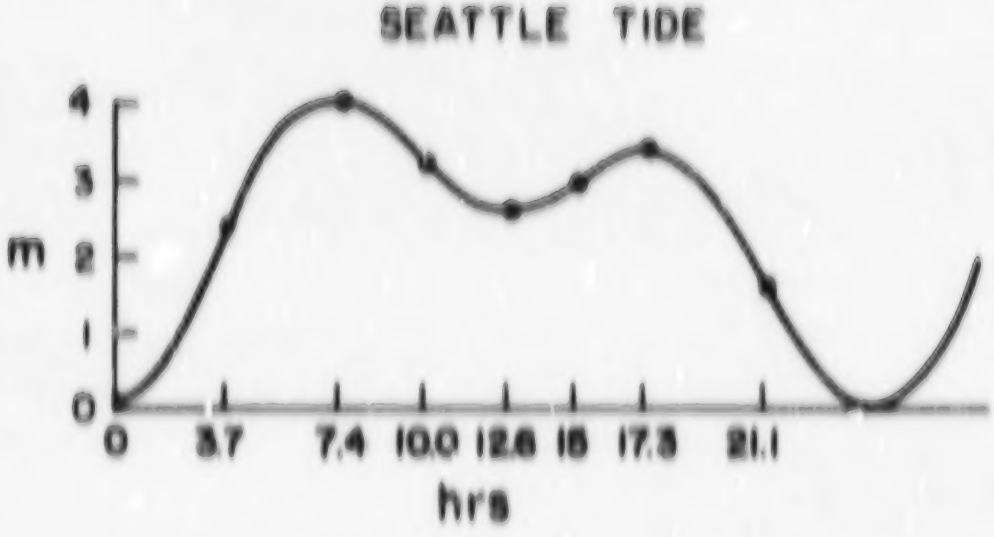

Fig. 18. Measured model tide at Seattle; the times correspond to the beginnings of each of the eight streamline photographs.

during the two high tides and the two low tides in the cycle, numerous eddies are present in many areas of Puget Sound. Some are formed behind the minor points, and others which were formed during the preceding flows around the major projections, are carried into mid-channel by the time of slack water. At slack water, a few of the channels still show evidence of residual flows. With the ebbs and the floods, major eddies exist only behind the larger promontories, and most of the remaining streamlines are directed nearly parallel to the shorelines of the channels. At the heads of some of the embayments and inlets, there is little indication of motion even during the major floods and ebbs. Other areas--such as the stretch between Deception Pass and Possession Sound--show motions which are less during the floods and ebbs than during the high and low tides at Seattle, indicating a phase lag in the flow characteristics.

One very important characteristic of the model is that the major circulation features--such as the dominant eddies and the direction of magnitude of the stream lines--are remarkably repeatable. This result was to be expected, of course; otherwise it would not have been possible to conduct a study of the periodic tidal circulation. It is encouraging, though, that the flow features which are random and would be expected to vary with each successive identical tide stage, are of a smaller scale than the dominant features in the tidal flow charts.

One of the objectives of this study was to identify areas in the model where there was very little tidal flow. For practical purposes, these areas were considered to be the ones where a two-second time exposure of the styrofoam particles did not produce an image with an obvious direction of movement. It appears, then, from the results that in areas such as Penn Cove, Holmes Harbor, Elliott Bay, Carr Inlet, the heads of Case Inlet and Dabob Bay, and the southern part of Hood Canal from the Great Bend to Lynch Cove, there is relatively sluggish flow at any stage of the tide. The results from very shallow areas may be in doubt because of experimental difficulties due to capillary action.

As for the remainder of Puget Sound (i.e., the major portion where we find significant water movement), we were interested in distinguishing regions

with flow characteristics which are similar across the channel from regions where the flow changes across the width of the channel. There are few locations that appear to have flows that are uniform across the channel at all stages of the tide. One of these locations is the central portion of Hood Canal. Another is the middle portion of Saratoga Passage. By far the larger part of the Sound is characterized by tidal flows which are not uniform across the channel. These latter flows fall into two categories: 1) those which are non-uniform at any instant of time across the channel but which might be more uniform if the higher frequency variations are removed, and 2) those which vary across the channel even if high frequencies are filtered out.

One major source of cross-channel variation is the system of eddies which covers much of Puget Sound during periods of slack water. Some of these eddies are obviously associated with nearby physical features in the shoreline or bathymetry, while other appear to be more randomly distributed. Quite possibly, if the motions of these eddies were averaged over a tidal day, some of them would show cross-channel uniformity, while others would show a variation in mean flow from one shore to the other.

There are two other obvious sources of cross-channel variability in the flow: curvature in the channel configuration and physical features which cause the ebb and flow patterns to be different. A striking example of the latter is seen in the portion of the Central Basin just north of Vashon Island. In that region, the channel configuration is such that floods tend to be directed into East Passage. Ebbs into this channel from Colvos Passage have greater flow speeds than the component coming from East Passage. The result of this higher velocity flow through Colvos Passage is that during slack water following the ebb in the rest of the system, a northward flowing core of water persists through the central portion of the channel west of Alki Point. This tends to bias the flow in that region to the north and, therefore, creates a flow which is not uniform across the channel. Similar results are likely to be found in other confluent regions with high flow velocities.

Three other features which were observed in the photographs of tidal currents are worthy of special mention. These include an apparent asymmetric flow around Vashon Island, a noticeable difference in the timing of the tidal currents between Deception Pass and Possession Sound as compared to the

currents in the rest of the area, and an interesting feature in the surface currents in Elliott Bay. As to the first of these, floods tended to be directed towards East Passage on the east side of Vashon Island, while stronger currents were found in Colvos Passage during ebbs (as already mentioned). The observations indicate that, during floods, southerly speeds in East Passage and Colvos Passage are comparable; during ebbs, the northerly speeds in Colvos Passage are larger; at high tide there is residual flood movement in East Passage; and at low tide there is residual northward ebb flow in Colvos Passage. The obvious interpretation of these results is that there is a clockwise flow around Vashon Island. Release of dye into the water around Vashon Island appears to confirm this interpretation.

Another flow feature that emerges from the photographs is that the timing of tidal currents in the Skagit Bay channel and in Saratoga Passage appear to be different from those in the principal channels of Puget Sound. The Deception Pass and Skagit Bay areas show little movement at times when flows in the main channels are near their maxima. This difference with respect to the major portion of the system is caused by a phase lag between tides in Rosario Strait and those in the vicinity of Skagit Bay. The phase lag is due to the greater transit time of the tide around Whidbey Island and produces a difference in water level between those two areas. Consequently, the currents are the result of a hydraulic head, which is not directly related to the current behavior of the main channel. Furthermore, these currents are strongly affected by the changing character of the tidal sequences.

Finally, it appears that, during floods, water is being drawn out of Elliott Bay around Duwamish Head and, during ebbs, water flows into Elliott Bay via the same route. Since the tide height in the bay is increasing during a flood and decreasing during an ebb, water must be flowing into and out of the bay at depth during those times. In the study described in the next section, it was found that surface waters do indeed exit via Duwamish Head during floods and enter there during ebbs. It was also found that there is inward transport of deep water during floods and that there is a small amount of surface water flowing into Elliott Bay during a flood along the east side of the bay. This flow is not evident in the tidal current photographs because of its low velocity.

6.3 DYE STREAM DISPERSAL CHARACTERISTICS IN THE PUGET SOUND MODEL

In these studies colored dye was injected continuously into the water at various locations, and the movement of the dye was recorded photographically on 16 mm motion picture film. Surface flows were observed by using a low specific gravity dye solution that initially would be retained in the near-surface layer. For locations at which dye was injected at depth or near bottom, the specific gravity of the dye solution was adjusted to be as nearly neutrally buoyant as possible. In many cases, vertical movement and mixing caused dye to be dispersed over an appreciable depth range. Vertical dispersion, however, is not readily apparent on the photographic record because the photographs were taken vertically from above the model. Where vertical movement is subsequently described, it is the result of visual observations made during the course of the run.

The motion of the dye was photographed with a Bolex 16 mm movie camera mounted directly above the model. Photographs were taken at approximately one frame per second, or with reference to the model time scale, one frame every 20 minutes of model time. Runs were continued for at least ten model days. For time reference, a moving tape showing the tide marigram, date, and time was also included in the photograph. The tide stage can be determined from that marigram which moves past an index mark at a rate equal to the model time scale.

Because of anticipated changes in the rate of mixing of water in Puget Sound as the tidal amplitudes change, studies were made during periods representing spring and neap tides. The period of May 1 through May 10, 1973, was chosen for spring tides, and that of October 3 through October 11, 1973, was selected for the neap tides. The tide marigrams at Seattle for these two periods are shown in Figs. 19 and 20, respectively. The tides for each complete month are included to illustrate the manner in which the tide character progressively changes.

To investigate the effect of different river discharge rates, runs for selected locations were made with rivers set at the lowest monthly average discharge and the highest monthly average discharge. Discharge rates for the eleven major rivers included in the model are listed in Table I. These flows have been adjusted to compensate for smaller streams and ungaged discharge into

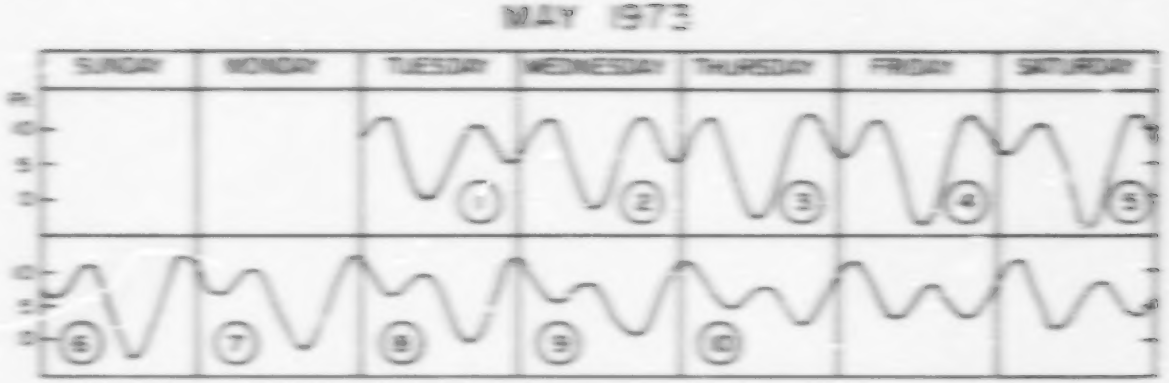

Fig. 19. Representative spring tides at Seattle (May 1973, days 1 through 10).

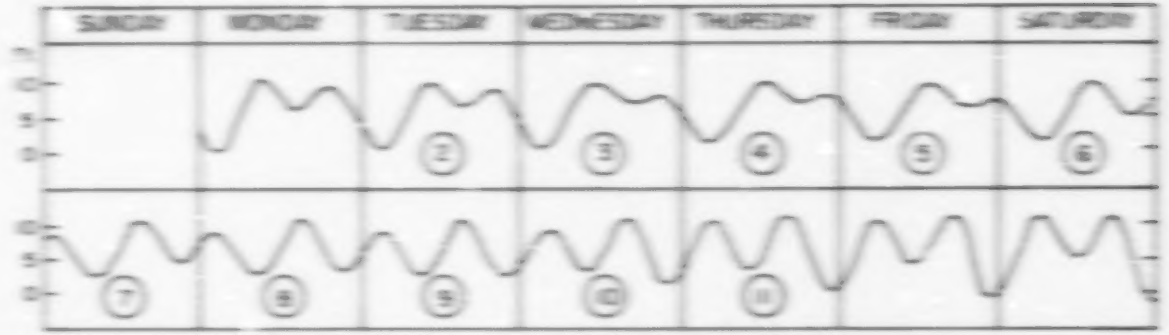

Fig. 20. Representative neap tides at Seattle (October 1973, days 2 through 11).

Table 1. Discharge rates for the major Puget Sound rivers.

River	Discharge Rate: Highest Month Average (m^3 sec^{-1})	Discharge Rate: Lowest Month Average (m^3 sec^{-1})
Skagit	1045	361
Snohomish	685	113
Stillaguamish	241	42
Puyallup	284	149
Duwamish	139	50
Nisqually	213	78
Skokomish	125	39
Cedar (Lake Washington)	85	31
Dungeness	34	10
Hamma Hamma	20	6
Duckabush	30	8

Note: These values are 15-year averages and have been adjusted for both ungaged flow and for discharge of the smaller streams flowing into the basins receiving the major rivers.

areas contiguous to the river drainage basins. It should be noted that short-period variation can result in both higher and lower rates than used in the study. Also, yearly variability may affect peak and minimum flows.

The locations for these studies were chosen partly because of practical considerations (potential pollution sites) and partly to obtain representation of different types of systems. West Point and Elliott Bay were chosen for intensive study; the first represents a deep inlet channel with bathymetrically induced mixing, and the other represents a quieter embayment at the head of an estuary. Both are potentially sites of environmental stress. In addition, studies were conducted at a number of bottom locations in Puget Sound because of their importance as dredge spoil sites. The locations of these sites are also shown in Fig. 15.

Because of the complexity of the bathymetry and channel configuration in Puget Sound, it is difficult to generalize about the dynamic behavior within the whole system. Even though one observes outward net transport in the upper layer and inward net transport at depth in most areas, local exceptions do exist. Although the details of circulation patterns depend upon locations, certain dominant features are observed for locations with similar topography.

Except for areas very close to river mouths with freshwater plumes, tidal currents usually are larger than the density-driven circulation in the model. The principal factors determining the characteristics of these strong tidal currents are shoreline configuration and bathymetry; their effects on the water movement may extend for distances of several kilometers. In a number of places, promontories or "points" extend into the main channel (Bush Point, West Point, Alki Point, Fulley Point), and tidal flow past these promontories results in the formation of large-scale eddies or gyres that alternate with ebb and flood currents. These eddies are very effective in promoting cross-channel transport of water. For example, an eddy formed downstream of a point may be carried toward midchannel when the tidal currents reverse. Usually this behavior will occur during each flood and ebb, and, while the basic pattern tends to repeat, the size of the eddy and it subsequent behavior will be influenced by the variable ranges of the successive tides. Occasionally, during periods of very small tides, such as may occur during neap tides, eddy formation may be weak or may not occur. This effect, somewhat modified, also

occurs at depth since surface features are reflected in the deeper bathymetry. The direction and mean speed of flow at a fixed depth has been observed to vary with the magnitude of river discharge. Furthermore, the behavior of the mean flow appears to depend to some extent on the tide type.

In the following paragraphs, we describe the general results from West Point, Elliott Bay, and the dredge disposal sites. The interested reader should refer to the 16 mm motion picture record for critical details.

West Point

At West Point, dye was injected into the water from three near-bottom locations on the eastern side of the channel. These positions, situated on the ridge or buttress extending into the water from West Point and at the surface, 73 m, and 165 m were chosen to simulate discharges above, at, and below the depth of the existing sewage treatment plant outfall (see Fig. 21). Studies were conducted for both spring and neap tides and at high and low river discharge over a total of 13 runs.

It was found that in most instances dye released at all three depths dispersed across the channel within a longitudinal distance from the injection site equal to two channel widths. This dispersion is due to the lateral motions induced by the protrusion of West Point into the channel and depends on the magnitude of the tidal currents. Spring tides result in greater lateral motions than neap tides. Dispersion near the surface was essentially in a horizontal plane; the large vertical density gradients effectively inhibited vertical mixing. At depth, the dominant mixing was roughly parallel to equal density surfaces, but mixing across density interfaces also occurred. Mean transport of the dye over 10 days was seaward at the surface and even at 73 m, but it was directed landward at 165 m. Daily mean transport deviated from the long-term mean pattern on some occasions possibly because of slow changes in the volume of water in the fjord from long period variables. For instance, there was no northerly surface transport during the first part of the neap tide period with low river runoff due to an apparent accumulation of water in the basin. There were also occasional variations in the transport which are presently unexplained. Qualitatively, larger mean transports were observed during high river discharge than during low river discharge.

The sharp protrusion of West Point into the channel, along with the relatively large tidal currents at the surface, result in frequent formation of clockwise and counter-clockwise eddies behind the point during ebb and flood tides, respectively. Upon reversal of the tide, these eddies would be advected into mid-channel. Also, because of the configuration of West Point and its associated bathymetry, which tends to accelerate the flows on the east side of the channel, the currents on that side were stronger than those on the west during both ebb and flood. Even though cross-channel mixing occurred regularly during the spring tides, the weaker currents accompanying neap tides were often insufficient to disperse the dye across the width of the channel before the dye concentration diminished to the point where it was no longer visible. There were also occasions during small tide ranges when the slower flows did not produce back eddies behind the point, but merely produced much slower flowing water in place of the eddies.

At 73 m, the combination of lower tidal velocities and more gradual curvature of the West Point buttress results in less turbulent flow along the sides. Whereas the point frequently sheds eddies in the surface currents, at 73 m a reverse flowing eddy is rarely developed. Even though the flow is apparently less turbulent at this depth because of the smaller channel width, dye was consistently mixed across the channel. The mean transport at this depth was northward, as in the surface, but it appears to be of lower magnitude.

The deepest discharge site at 165 m also showed apparent cross channel motions; though, here, like the runs made at mid-depth, distinct eddies were not found. Unlike the two shallower discharge sites, the mean transport of dye released at this depth was landward to the south.

Elliott Bay

Elliott Bay, in contrast to West Point, is a relatively quiet body of water, closed at one end with a river discharging into its head. The circulation in this bay is complicated due--among other things--to the fact that it is joined to the side of a major channel, has two distributaries of the Duwamish River discharging into it, and has a pair of submarine canyons located on either side of it. In order to describe some of the features of the circulation and to study the residence time of water in Elliott Bay, dye discharges

were injected into six different locations within the bay (see Fig. 31). Three near-bottom sites were chosen: one in each of the two submarine canyons and one at a slightly greater depth (Duwamish Head dredge disposal site). In addition, three near-surface discharge sites were also chosen: one in the Duwamish River, one at the southern end of the Seattle waterfront, and a third one at Smith Cove on the northern end of the waterfront.

The results of the studies at these sites, which were conducted for a combination of river states and tide types, provide a set of descriptions showing dye distributions of some complexity. On the average, dye injected at depth was carried inward and upward until it reached to within about 37 m of the surface; whereupon, it turned seaward and was ultimately dispersed either past Smith Cove or around Duwamish Head. Dye which upwelled through the West Waterway was always dispersed around Duwamish Head. Dye injected in the eastern submarine canyon and that introduced at the waterfront normally was removed via the Seattle waterfront even though it did disperse throughout Elliott Bay and exit via Duwamish Head on some occasions. Dispersal of dye within Elliott Bay can be rather slow with observed residence times of up to 1.0 days for dye flowing north along the waterfront. Once the dye in the bay passes an imaginary line extending roughly from Smith Cove to Duwamish Head, it was dispersed more rapidly by the strong tidal currents in the Central Basin of Puget Sound. As expected, the accumulation of dye in Elliott Bay was greatest during low river runoff.

The limited number of observations, the variability in the rate of dye discharge, and the differing distribution of water between the east and west channels of the Duwamish River preclude our making definitive statements about circulation patterns in Elliott Bay. One possible description of the circulation in the bay, which is consistent with the observations, is as follows: Generally, we observe a standard estuarine gravitational convection pattern with saline water intruding at depth and a brackish zone flowing out near the surface. Because of the distributed source waters and the width of the bay, the surface zone in Elliott Bay consists of two flows, with the core of the discharge from the higher runoff West Waterway flowing along the west side of the bay and the core of the much lower discharge East Waterway moving along the Seattle waterfront. Superimposed on the mean circulation is a

tide-induced circulation. On flood tides, the circulation is clockwise with water moving into the bay in the east and flowing out around Duwamish Head. During ebb tides, the directions are reversed, and a counter-clockwise flow prevails. Because of the configuration of Elliott Bay relative to the Central Basin, the flow in Elliott Bay is stronger during flood, and there is net clockwise, mean tidal flow. The resultant of the tidal and gravitational flow is a net outward flow at the surface with more water flowing out around Duwamish Head than past Smith Cove. Whether water from the eastern part of the bay flows north along the Seattle waterfront or is incorporated into the flow past Duwamish Head depends upon the relative magnitude of the river discharges and tidal flows. Water is most likely to flow out past Smith Cove for combinations of low tidal currents and high river discharges. Conversely, for high tidal currents and low or no river discharge, there is most probably no outward transport past Smith Cove.

The results from the near-bottom injection sites in the eastern canyon (Elliott Bay 1, 119 m), in the western canyon (Elliott Bay 2, 82 m), and at depth (Duwamish Head dredge disposal site, 137 m) are consistent with the general features of the circulation as proposed in the last paragraph. Observations from the Duwamish Head disposal site showed an upwelling of the dye and subsequent dispersion from the outer parts of Elliott Bay into the Central Basin. Because of the low dye concentrations, it was difficult to describe the surface behavior of the dye from this injection site. The two sites in the submarine canyons showed the expected upwelling of water from the bottom into the near surface layer. The dye appeared routinely to reach to within 37-55 m of the surface before being transported outward in the surface flow. Dye that remained in Elliott Bay for extended periods of time had the chance to adjust further its density to that of the near surface water and was observed within 7-11 m of the surface. Dye originating in the western canyon was consistently swept outward past Duwamish Head. Dye injected into the eastern canyon was removed along the Seattle waterfront during high river runoff and was observed to disperse throughout Elliott Bay and to be dissipated around Duwamish Head during neap tides and low river discharge. Similarly, for low river discharge and spring tides, the dye which reached the surface was swept around the bay and out past Duwamish Head.

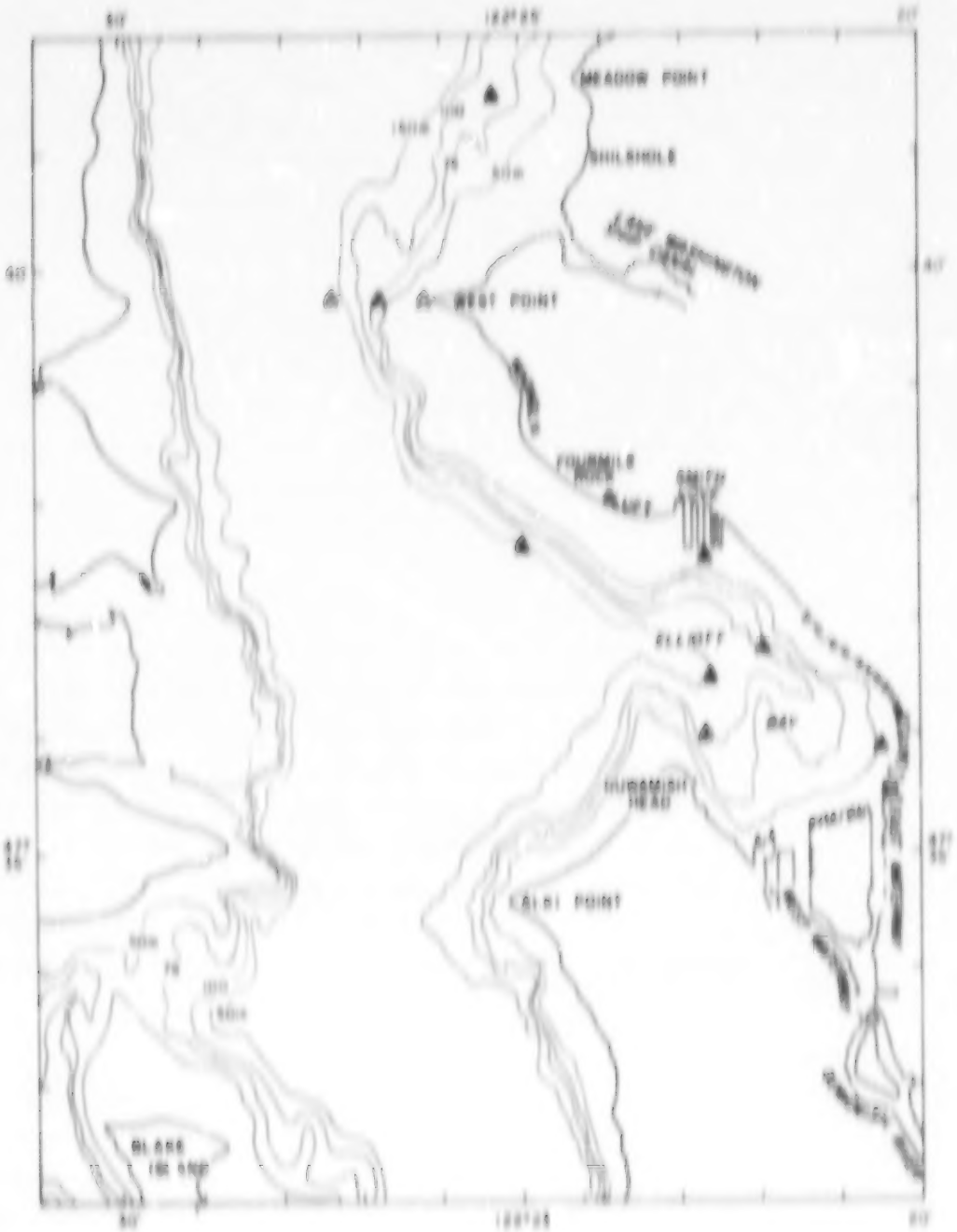

Fig. 21. Dye discharge locations near Seattle; solid triangles are dredge disposal sites.

The near-surface discharge sites, like the near-bottom ones, corroborated the proposed description of the circulation. Dye introduced into the Duwamish River and dye injected along the southern end of the Seattle waterfront behaves in a predictable manner. In all cases, river water discharging from the West Waterway of the Duwamish into the western half of Elliott Bay flowed along the western shore and was dispersed around Duwamish Head. For neap tides with the related weaker tidal currents with both high and low river discharge, water from the East Waterway flowed along the waterfront and past Smith Cove. With spring tides and low river discharge, the average tidal current was stronger along the eastern shore than the river-induced flow; so, water from the East Waterway which migrated north along the waterfront was incorporated into the tidal flow and was swept back into the bay until it merged with that from the West Waterway and ultimately dispersed around Duwamish Head. With spring tides and high river discharge, there was not enough dyed water flowing from the East Waterway to determine whether the river water flowed out past Smith Cove or Duwamish Head. Given the other observations of the Duwamish flow, either case would seem reasonable. Water injected at the Seattle waterfront behaved in a similar manner. For neap tides, dye was transported north along the waterfront and past Smith Cove. For spring tides and low river discharge, as with Duwamish River water, the northerly moving dye was incorporated into the clockwise flow and finally carried around the bay and out past Duwamish Head. In this case, the results from the spring tide, high river discharge run showed dye moving north and out past Smith Cove.

Near surface injections were made at Smith Cove for both tide types and low river discharge. This dye was mainly swept along by the stronger currents of the Central Basin and was dispersed both around Alki Point and around West Point. However, there was some dye intrusion part-way into the central part of Elliott Bay. Since the core of the river discharge mainly held to the sides of the bay, it is reasonable to find that water from Smith Cove intruded most strongly into the central part of the bay.

Dredge Disposal Sites

Model studies of the dredge spoil disposal sites were designed to investigate the currents in the vicinity of the sites as well as the pathways taken by the

water after it leaves the immediate area. At each of the sites, dye was injected into the water close to the bottom. It must be stressed that these studies do not address the question of movement of the spoils themselves. However, any attempt to predict the movement of the dredge spoils, both as they were settling towards the bottom and after incorporation into the sediment, must be based on a knowledge of the water movement nearby.

The results of the near-bottom dye injections may be separated into three categories. Sites located on the sides of the channels, such as Fourmile Rock, Shilshole, and Everett, have circulation patterns parallel to the bottom contours. Duwamish Head and the two locations in Commencement Bay display a more typical estuarine-type circulation with a tendency for the bottom water to flow landward before being incorporated into the near-surface layer and dissipated. Finally, the site at Dana Passage shows high dispersal of the dye because of the turbulent flows through that narrow passage. There, even though the accumulation of dye at the discharge site is negligible, traces of dye could be seen in all of the nearby inlets. Because of the small effects of changing river discharge on the near-bottom flows, the studies at the dredge disposal sites were conducted for high river discharge only but for both spring and neap tides.

Results of the study at Duwamish Head have already been discussed briefly in the description of Elliott Bay. The two sites in Commencement Bay (Fig. 5) located in the inner (110 m) and outer (165 m) parts of the Bay differ from Duwamish Head (and other Elliott Bay locations) most notably in having larger tidal excursion and mixing. There, especially for spring tides and the outer site, dye from the injector was often drawn into the main channel and dispersed within one tide cycle. This enhanced circulation and mixing is due to the bathymetry and shoreline of the area adjacent to Commencement Bay. Transport in East Passage, just outside of the Bay, is unusual in that it is southward both at depth and at the surface.

During floods, water in East Passage moved south as surface water in Commencement Bay, and deep upwelled water in this area moved into and through the Tacoma Narrows. Only very weak southerly currents developed in Colvos Passage at this time. During ebbs, the circulation became more complex because the

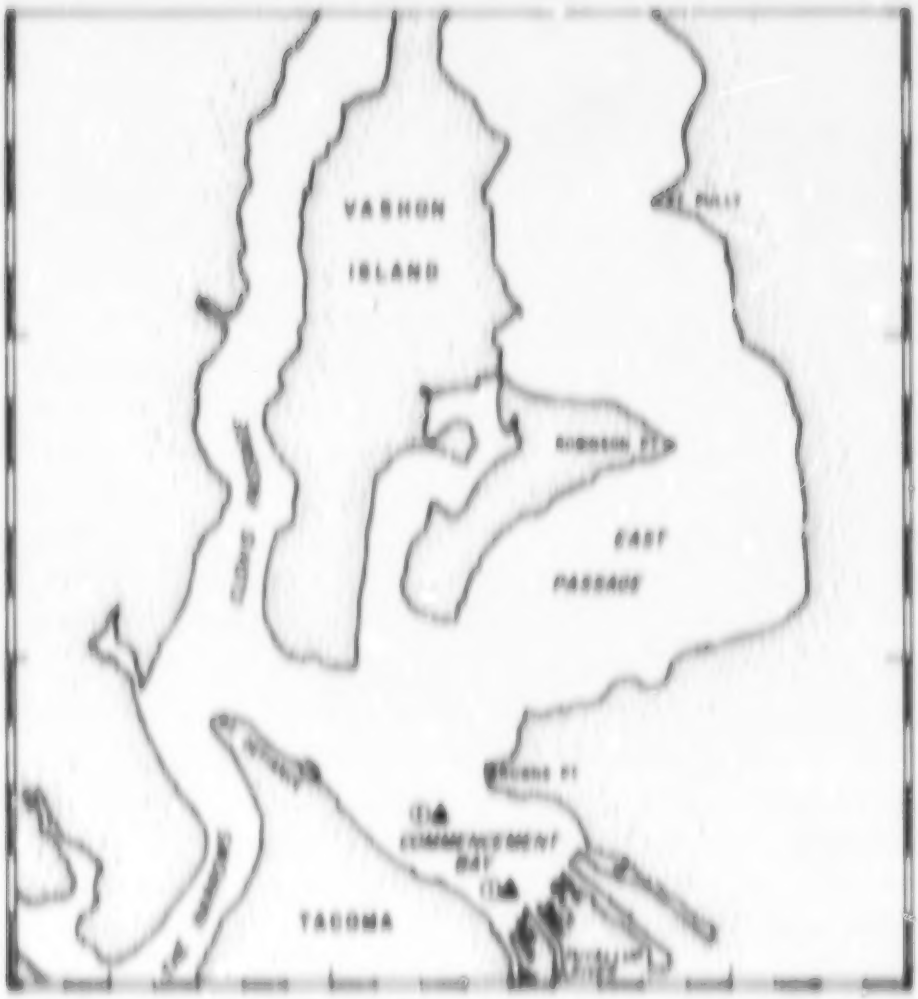

Fig. 22. Dye discharge locations at two dredge disposal sites in Commencement Bay.

configuration of the Narrows directed flow from that channel toward the southern end of Colvos Passage. During the first part of large ebbs strong turbulence from the Narrows was diverted eastward around the southern end of Vashon Island. This turbulence was carried into Commencement Bay where it resulted in strong mixing within the entire water column. As the ebb continued, a strong northerly flow in Colvos Passage developed that carried the major part of the discharge from the Narrows. The strongly turbulent flow eastward into Commencement Bay decreased as the flow through Colvos Passage increased. Water in Commencement Bay rarely was carried north in East Passage for more than 4 mile or two beyond Browns Point. The result of these flow characteristics was a net clockwise circulation around Vashon Island.

Dye injected during spring tides at Commencement Bay--Site One, located near the head of the bay, produced a filamentous cloud that reached inward to the head of the bay at depth and outward toward the mouth opposite Browns Point. The outward edge of the cloud was rapidly distorted by flood flow past the shoulder of Browns Point and to a greater extent by the turbulence resulting from the strong outflow from the Narrows during the previous ebb. Periodic upwelling along the steep slope at the head of the bay was observed and appeared to reach its maximum excursion at the end of the flood. During ebbs, the upwelled water tended to subside and move away from the head of the bay. Horizontal excursion during the large tide ranges was about one mile. The upwelling behavior was primarily oscillatory rather than continuous. Upwelling of deep water along the shoaling bottom leading to the Narrows occurred during floods and carried dye from the outer portions of the accumulated cloud into the channel, and the dye was subsequently dispersed by the turbulent flow through the Narrows.

In contrast to spring tides, neap tides were markedly less efficient in dispersion and transport of dye at this site. Dye tended to accumulate as an irregular cloud at depth near the injection site, with small oscillations of about 0.5 km occurring during the larger ranges of the early part of the period. A small amount of turbulence and upwelling resulted in some dispersion toward the head of the bay and outward to form an elongated cloud about 2.3 km long.

Appreciable outward transport toward the Narrows did not occur until later in the time period when the character of the tidal cycle produced more nearly equal semidiurnal ranges. By October 7 or 8, a filament of dye began to be carried outward at depth along the southwest side of the bay toward the Narrows during flood tide. By October 11, a thin filament and low concentrations were visible about 5.5 km from the site. Visible amounts of dye were not observed reaching the north entrance to the Narrows by the end of the observation period. The principal accumulation was still present as an irregular cloud extending about 1.4 km from the site.

Commencement Bay--Site Two is located at the mouth of the bay so that the major difference between it and Site One is the increased mixing at this outer location. During spring tides, dye from this site was dispersed much more rapidly than that from Site One. Movement inward toward the Narrows and upwelling at the head of the bay was quite evident during the flood tides at the beginning of the period. Onset of rapid dispersion by the turbulent front associated with ebb flow from the Narrows was usually sudden.

In general, during neap tides the dye formed a small filamentous cloud that oscillated between the head of the bay near Site One and the base of Browns Point. During the first few days of this period, the dye cloud was about 2 km long and 0.5 km wide, with its major axis along the axis of the bay. At the time of high tide, it was centered on the injection site. A very thin and faint filament was carried around the base of Browns Point where it was dispersed rapidly by the main channel flow during flood tide.

Dispersion of the dye was so intense, even with neap tides, that dye was almost undetectable more than about 3.5 km from the site towards Point Defiance. Upwelling of dispersed dye near the head of the bay occurred but was most evident during the latter part of the period when the character of the tides had changed to more nearly equal ranges.

As mentioned earlier, dredge disposal sites located on the sides of relatively straight portions of the main passages had current patterns which tended to carry the injected dye along a uniform depth contour line. In actuality, the dye was carried along the contour lines, undisturbed, for some distance, and then was dispersed as it became mixed into more turbulent flow. At Fourmile

Rock (Fig.19), dye was injected at a depth of about 121 m and formed a narrow band at this depth which extended from West Point to near Smith Cove. During ebbs, dye which reached West Point was dispersed by the turbulence generated there. On floods, dye reaching the vicinity of Smith Cove was subjected to mixing and continued on as a much lower concentration dye cloud. This cloud continued southward until it was ultimately dispersed by mixing around Alki Point. On some occasions, part of this cloud drifted into the eastern canyon of Elliott Bay where it became sufficiently diluted such that it could not be traced further. In general, the difference between spring and neap tides was only in the larger excursions which were associated with spring tides.

The dredge disposal site at Shilshole (Fig. 21) is located in about 79 m depth. The main concentrations of dye were observed between Meadow Point to the north and West Point on the south. Because of the eddies formed behind these two points, there was more vigorous mixing even in this region so that there was less buildup than at Fourmile Rock. During spring tides, the dye was normally transported toward the south where it was dispersed around West Point. For neap tides, there was a more northerly transport with dispersion around Meadow Point. However, during the later stages of the neap cycle, the mean transport swung to the south.

For spring tides, the largest dye accumulation remained between Meadow Point and the entrance to the Lake Washington Ship Canal. Dye was carried by floods as much as two miles south of West Point. During ebbs, dye was transported about 1 km north of Meadow Point. At the same time, the eddy forming off West Point carried filaments of diffuse dye closer inshore in the Shilshole bight.

During the neap tide period, the principal accumulation was in the area between the injection site and the deep shoulder of Meadow Point. Although successive ebb tide ranges during this time were small, the flow picked up portions of the dye cloud and carried them 4 km northwest of the injection site. Dye could be traced nearly 5.5 km beyond Meadow Point. Late in the neap tide period, with the tides changing to more nearly equal semi-diurnal, there was increased flow to the south and dye was dispersed around West Point.

Of the three sites located on the sides of passages, Everett (Fig. 23) at 110 m had the least local mixing. The dye, discharged at depth, moved slowly in

Fig 23. Dye discharge location at the dredge disposal site near Everett.

the low tidal currents and slowly rose to about 27-33 m. During ebbs, the dye was carried to the southwest and some of it was dispersed around Elliott Point. During floods, dye was carried into Port Gardner, around the outer edge of the Snohomish River delta and across the mouth of Port Susan. Turbulence associated with flow across the Snohomish River delta and at the mouth of Port Susan slowly dispersed the dye before it was finally transported into Possession Sound. In general, the flow characteristics were similar for spring and neap tides, with the expected lower mixing and lesser tidal excursions being associated with neap tides.

Of the dredge disposal sites studied, Dana Passage (Fig. 24) with a bottom depth of about 18 m was by far the shallowest site as well as the location with the strongest tidal currents. Because of this, there was no accumulation of dye at the injection site, and shreds of dye were carried on floods into Henderson, Budd, and Eld inlets. During ebbs, the dye was generally transported toward the Tacoma Narrows though some of it was deflected into Case Inlet. There was no noticeable difference in the distribution of the dye between spring and neap tides since the currents were very strong in both cases.

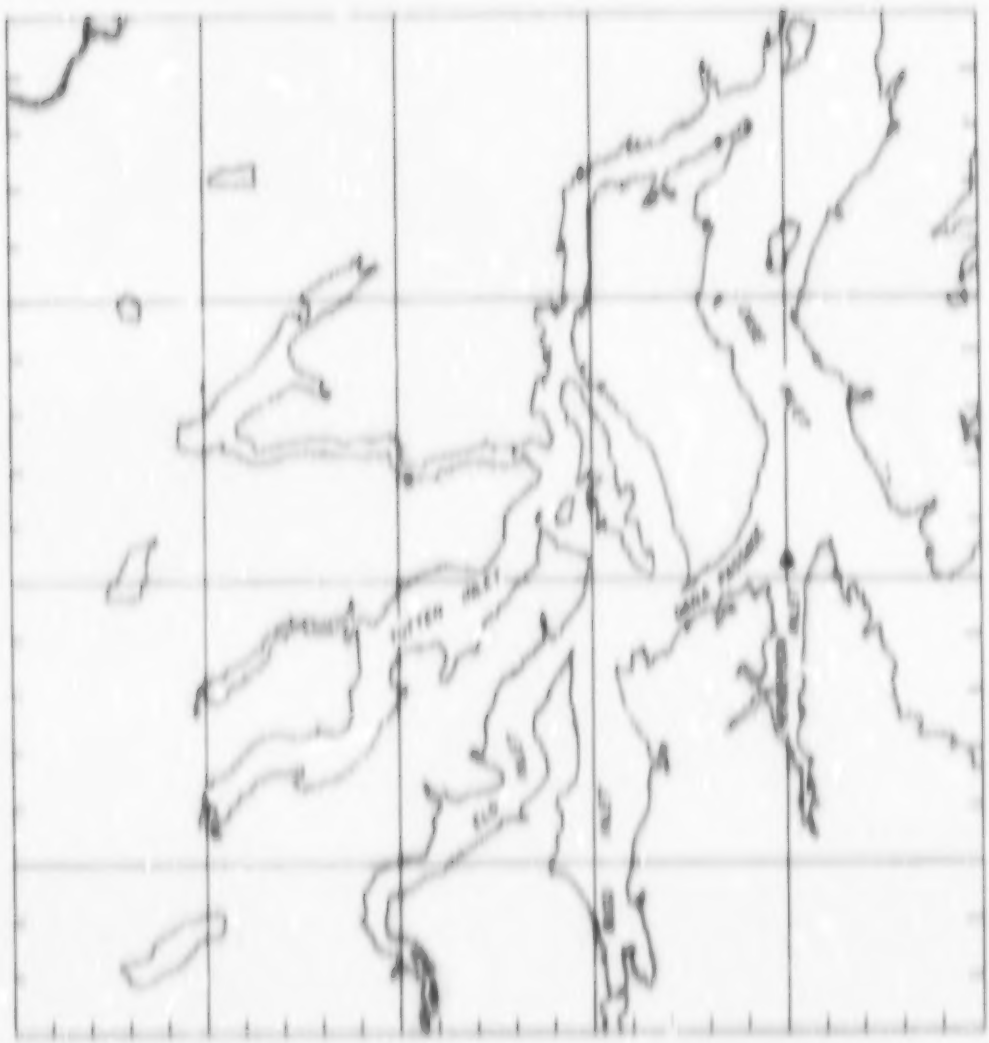

Fig. 24. Dye discharge location at the dredge disposal site in Dana Passage.

SECTION 5

NUMERICAL MODEL OF PRIMARY PRODUCTION IN PUGET SOUND, WASHINGTON

The overall objective of this phase of the project was to conduct a quantitative investigation of relationships between the growth of phytoplankton, and climatic and hydrodynamic conditions in a deep, temperate inlet with marked tides, as exemplified by Puget Sound, Washington. A fully detailed paper describing the results of the investigation has already been published (Winter et al., 1975) so that only the highlights of the primary production model need be summarized here.

As mentioned in Section 3, gravitational convection in a deep inlet, such as the central basin of Puget Sound, is characterized by a near-surface brackish water zone of many meters thickness flowing seaward over a deeper, landward-moving zone of salt water from the sea. Early qualitative observations of primary production in deep inlets suggest that phytoplankton growth is closely coupled to estuarine circulation as well as to the physical and chemical properties of the water. Under conditions of moderate stability, when insolation is adequate and the brackish zone of the inlet is not excessively turbid, algae may grow with sufficient vigor to exhaust the surface zone temporarily of plant nutrients. However, turbulent entrainment of nutrient-rich oceanic water from depth will tend to replenish the supply of these ions. On the other hand, cells growing near the surface are only temporary residents of the near-surface zone since they are advected persistently seaward, on the average. At the same time, the estuarine mechanism will resupply the near-surface zone with viable cells from depth. Some fraction of this "seed stock" may originate external to the inlet, entering the inlet with the intrusion of oceanic water at the mouth; the remaining fraction may consist of cells formerly growing in the surface zone, which have sunk or were mixed to depth in the vicinity of a sill and were subsequently carried landward with intruding saline water.

The principal objective of this work was to examine quantitatively the relationships between gravitational convection and other environmental factors and primary production in deep inlet environments. The central basin of Puget Sound, Washington, was used as an example. Puget Sound, as a whole, consists of a complex system of deep inlet basins and channels which constitutes the southern terminus of a more extensive system along the northeastern Pacific coastline from Washington northward to Alaska. The Sound as a whole communicates with the Pacific Ocean by way of the Strait of Juan de Fuca to the north (Fig. 25). The principal entrance to the Sound is through Admiralty Inlet. The intensity of the incursion of oceanic water through the channel at Admiralty Inlet is determined partly by tidal characteristics and partly by the rate of fresh water input to the Sound.

Throughout all seasons of the year, the principal basins of Puget Sound exhibit some degree of stratification. The density structure is determined primarily by salinity differences between brackish near-surface zones and deeper zones of more saline oceanic water.

The tides in Puget Sound are of the mixed type with a progressive increase in range from Admiralty Inlet to the inner regions. In the vicinity of Seattle, the mean and diurnal tidal ranges are 2.0 m and 3.5 m, respectively. In the neighborhood of the sill at Admiralty Inlet, strong turbulence and high tidal currents (up to 5 knots) are the rule. Elsewhere, throughout the open water of the Sound, tidal current speeds are usually less than 1 knot.

The principal nontidal circulation mode in Puget Sound is gravitational convection, induced by freshwater runoff. The greatest amounts of fresh water are supplied to the Sound by rivers along the northeastern shore. During the spring and early summer, runoff into the central basin is derived largely from melting snow in the surrounding mountains rather than local rainfall.

Phytoplankton is found in appreciable concentrations (usually > 0.1 mg Chl a/m^3 even at depth) in nearly all parts of Puget Sound throughout the year, but the algae proliferate during the spring and summer months. Although field studies of phytoplankton production have been performed in a few locations in Puget Sound and the San Juan Archipelago, the present investigation is based largely upon hydrographic and biological data acquired during a Puget Sound field study

Fig. 25. Map of Puget Sound.

initiated in 1961 by G. C. Anderson and K. Ranse. The field work was motivated partly by the fact that in the early 1960's the municipality of metropolitan Seattle (METRO) began the construction of a central sewage treatment plant with a large outfall at West Point on the eastern shore of the central basin (Fig. 25). The observational program was undertaken to establish baseline conditions of environmental and biological variables, as well as to investigate primary production in Puget Sound.

Measurements were taken at two stations, one near midchannel in the central basin off Seattle, the other one located in the southern part of the Sound (Fig. 25). From September 1963 through December 1965, the stations were visited approximately biweekly to observe insolation, standard physical and chemical water properties, and concentrations of chlorophyll a and zooplankton. Measurements were also made of the rate of carbon uptake by phytoplankton in water samples drawn from several depths. The carbon uptake rates above the 1% light depth at the northern (central basin) station were 460 and 470 g C m^{-2} yr^{-1} in 1964 and 1965, respectively, which is extraordinarily high for an unpolluted temperate site. In contrast, the uptake rates in the southern Sound for the same years were 270 and 280 g C m^{-2} yr^{-1}, respectively.

The data indicated that primary production at the southern station was fairly uniform from March through September. However, the observations in the central basin showed that the annual cycle of phytoplankton growth was dominated by a number of intense blooms between early May and September. Moreover, the algal concentrations were changing drastically within time periods shorter than the sampling interval. Therefore, during some of the spring months of 1966 and 1967, the same parameters were studied on an almost daily basis at the central basin station.

The results of observations acquired at the central basin station during the springtime cruises in 1966 and 1967 are summarized in Figs. 36 and 37, respectively. The figures present the data in the form of isopleth diagrams showing the time and depth variations of salinity, temperature, density, oxygen saturation, phosphate, silicate, nitrate, chlorophyll a, and carbon uptake rate from April to June 1966 and in April and May 1967. A detailed account of the field measurements and methods, together with a description of supplementary observations, is available in Winter et al. (1975).

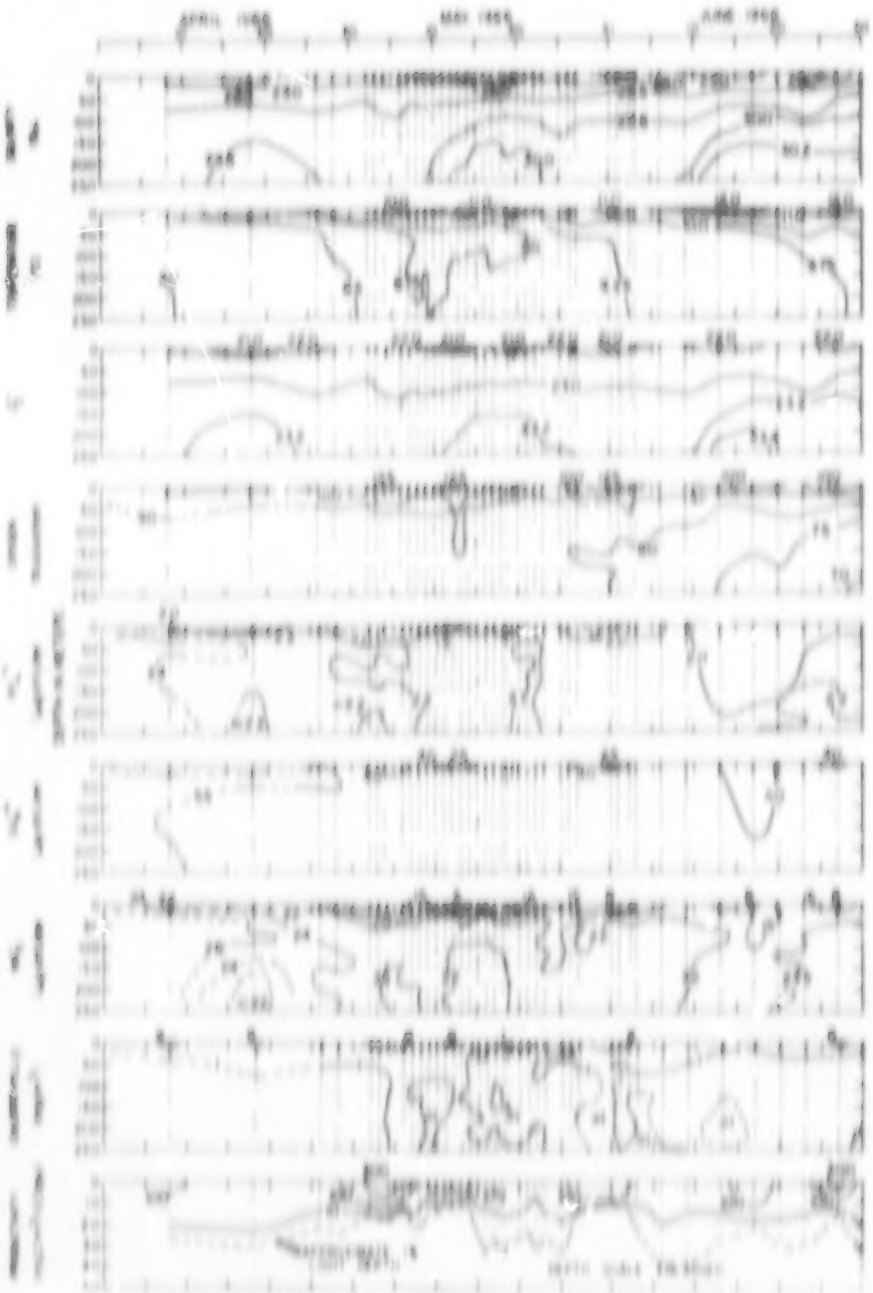

Fig. 28. Variations of salinity, temperature, density, oxygen saturation, phosphate, silicate, nitrate, chlorophyll *a*, and carbon uptake rate at Station I, April to June 1966.

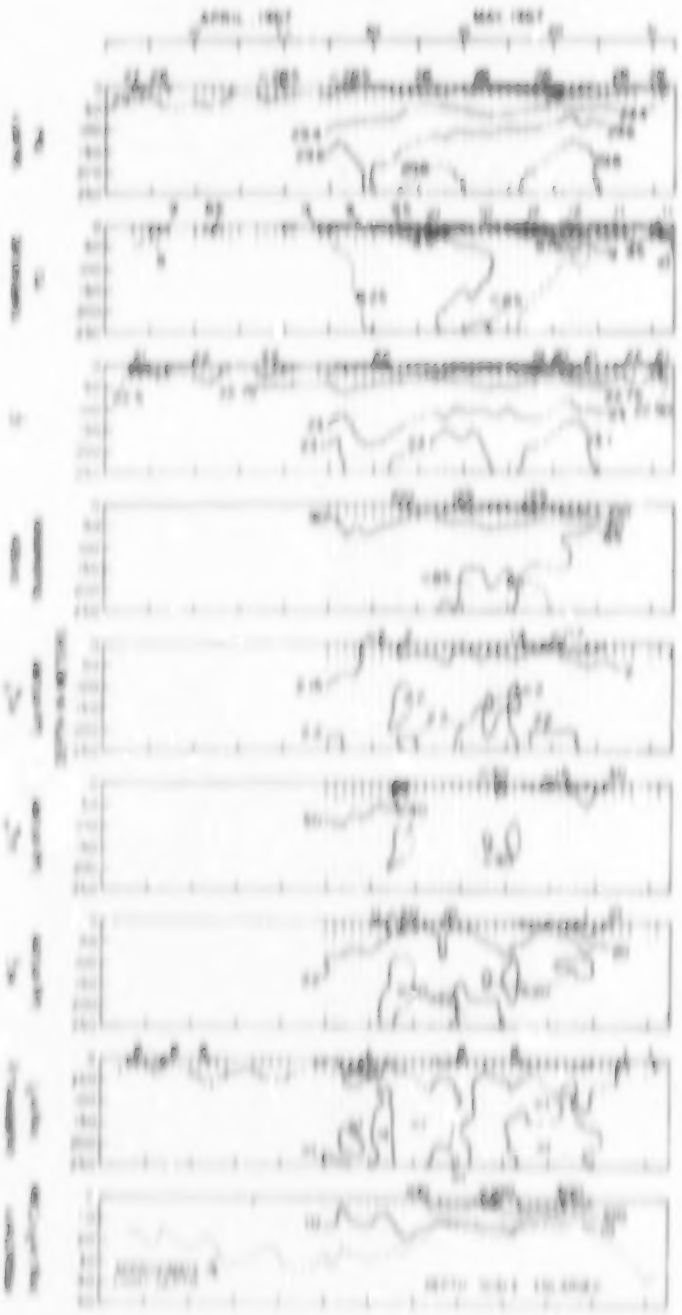

Fig. 27. Variations of salinity, temperature, density, oxygen saturation, phosphate, silicate, nitrate, chlorophyll *a*, and carbon uptake rate at Station 1, April and May 1967.

The quantitative investigation of deep inlet primary production processes was concerned specifically with the dynamics of springtime phytoplankton blooms and the variation in productivity, as exemplified by the central basin data. The principal investigative tool was a numerical model in which the hydrodynamical conditions were represented by an approximate similarity analysis of the gravitational convection mode of inlet circulation. Algal concentration was represented as a continuous function of space and time in the model, which ascribed changes in phytoplankton density to variations in photosynthetic and respiratory activity, algal sinking, grazing by herbivores, and to mixing and advection. As shown below, computations adequately reproduce the principal features of phytoplankton concentrations observed during 75 days and 35 days in the springtime months of 1956 and 1967, respectively. Moreover, by means of numerical experiments, it was possible to assess the relative importance of various processes which govern the level of primary production in Puget Sound.

The analysis of gravitational convection in the central basin has already been described in Section 3 of this report. However, some amplification may be in order before describing the numerical model of primary production. It is appropriate to begin with a presentation of certain additional hydrographic information relevant to the nontidal circulation mode. Consideration is restricted to a segment of the central basin which is 30 km in length, bounded at its southern end near Blake Island and at its northern end near the southern tip of Whidbey Island (Fig. 25). This choice of segment boundaries reflects the fact that different sections of the Sound north of the Tacoma Narrows are characterized by different flow patterns. The central basin, as defined herein, constitutes an inlet segment characterized by the same general type of circulation pattern and hydrography. On the average, a significant fraction of the freshwater discharged from southern Puget Sound and the Puyallup River appears to enter the central basin near Blake Island, via Colvos Passage. The northern terminus of the segment marks the confluence with Possession Sound which carries freshwater from three of the largest rivers in the Puget Sound region.

The coordinate used in this discussion has its origin at the surface at the location of Station 1 near Seattle. The x-axis extends horizontally along the

axis of the central basin and is positive seaward; the z-axis is directed positive downward. The main channel of the central basin is idealized as a deep inlet segment sufficiently narrow and straight to preclude the occurrence of large cross-channel variations in the average flow. Although the width of the segment is somewhat variable due to irregularities in the coastline, the effective main channel breadth at Station 1 is taken to be approximately 5 km.

Fresh water introduced into the central basin segment at its southern end consists of runoff from the Puyallup River drainage basin and the drainage basins south of the Tacoma Narrows. In addition, the central basin receives fresh water directly from the Duwamish and Lake Washington drainage basins, and distributed runoff from coastal land along the length of the segment. Daily gaging station data for the spring months of 1966 and 1967 were used to estimate the temporal variations of the cumulative fresh water runoff rate R (m^3/sec) in the central basin. Three-day averages of the hydrographs were performed to simulate the smoothing effect of mixing in the vicinity of the river mouths. The gaged discharge from each of the drainage basins was corrected to account for ungaged area. Finally, as in the case of Hood Canal, described in Section 3, the longitudinal distribution of cumulative runoff R was assumed proportional to cumulative drainage basin area. In the absence of turbulence measurements in Puget Sound (and hence direct descriptions of the turbulent transport of momentum and salt), it was necessary to draw upon estimates of turbulent processes in other deep, stratified inlets (Winter, 1973). It was speculated that in Puget Sound tides play a more important role than winds or river discharge in providing energy for turbulent mixing in the central basin. For Canadian fjords, Trites (1955) suggested that changes in mixing intensity might be related to changes in the mean tidal velocity or its gradient in some nonlinear fashion (for example, to its square). Average values of the vertical eddy diffusion coefficient A^z in the surface zones of several inlets were estimated to be in the range of 1 to 10 cm^2/sec. Thus, for the central basin, the simple working assumption was made that the day-to-day change in the mean intensity of turbulent salt flux was proportional to the square of the maximum tidal range, with an average value of about 3 cm^2/sec between spring and neap tides. Comparisons of calculations based

on this assumption and hydrographic data from the field tend to support the notion of a general dependence of mixing processes on tides, although the exact nature of the dependence is probably not accurately represented.

In the case of the central basin of Puget Sound, the seaward increase in surface salinity β_0 is rather slight and is sometimes obscured by the presence of partially unmixed lenses of fresh water which originate from river mouths, following freshets. On the average, however, the salinity β_0 over the segment will be determined by mixing of fresh water runoff at the river mouths in the major embayments, and by the cumulative runoff rate R_D. In practice, the latter can be regarded as the principal factor determining the fractional salinity excursion defined by Eq. (24)

$$a_D = (\beta_m - \beta_0)/\beta_m$$

where β_m is the salinity at depth in the incursion zone. As a first approximation, the fractional salinity excursion a_D can be expected to vary in time primarily in response to temporal changes in R_D, and secondarily to changes in wind-induced mixing, turbulence at depth, and mode of introduction of the runoff.

A study of the salinity changes at depth at Station 1 showed that between the lower boundary of the euphotic zone (which varies from 15 to 30 m) and the still depth (50 m), the seasonal increase in salinity was fairly small over the observation periods, being somewhat less than 0.5 parts per thousand. In the numerical study of phytoplankton growth described below, the lower boundary L of the model domain is 30 m. This value was chosen since it corresponds to the greatest euphotic zone depth and also lies within the upper portion of the deeper saline incursion zone most of the time. For the purpose of calculating the velocity field of the gravitational convection mode by the similarity analysis described in Section 3, it is sufficient to assume that the salinity at still depth (about 50 m) is constant and equal to the approximately seasonal averages of 29.4 and 29.2‰ in 1966 and 1967, respectively.

With the aforementioned hydrographic data and topographic idealizations, self-consistent quantitative estimates were generated of gravitational convection in the central basin for the spring months of 1966 and 1967, by means of the approximate similarity analysis described by Winter (1973) and summarized in Section 3. Calculated results were compared with measured salinity profiles at various times during the springs of 1966 and 1967. The data periods were chosen to cover the broad range of runoff conditions encountered during the observation periods. It should be noted that the idealized circulation analysis implies that changes in the non-tidal circulation component reflect variations only in tidal amplitude and runoff intensity. Since time-smoothed runoff data and day-to-day changes in tidal amplitude excursions constitute the input data to the analysis, the calculated density structure and velocity fields over the basin segment do not show large changes on consecutive days. In most cases, fair agreement was achieved between the calculated salinity profiles and the observed salinity at Station 1.

The velocity components u and w are calculated from the same analysis; the calculated time-mean outflow at the surface agrees well with data from the few available measurements in Puget Sound made by Paquette and Barnes (1951) and by Cannon and Laird (1972). It is difficult to determine experimentally the depth at which the horizontal component of current reverses sign because the non-tidal velocities above and below that depth are small compared with tidal velocities. As noted in Section 3, the calculated depth of no mean motion in the central basin is somewhat more shallow than that inferred by Paquette and Barnes, but is the same order as that observed by Cannon and Laird when runoff is low or moderate.

A convenient measure of phytoplankton standing stock is the amount P of chlorophyll a in a cubic meter of water. In the model, P is taken to be the dependent variable of a partial differential equation which expresses the time rate of change of P as the resultant of changes due to transport by turbulent mixing and advection, photosynthesis and respiration, sinking, and grazing by herbivorous zooplankton. Although the effects of certain short-time scale flow phenomena on algal dynamics are neglected, the option is retained of examining the response of the algal community to diurnal and day-to-day changes of

available light. For this reason, the time variation of light intensity is included explicitly in the expressions for photosynthetic and respiration rates.

Under the hydrographic conditions described above, changes in momentum and salt concentration produced by longitudinal mixing are small compared with variations associated with vertical mixing and advection. The assumption is made that the turbulent transport mechanisms of suspended and dissolved substances are the same, and, therefore, the turbulent flux of phytoplankton can be represented by the product of the eddy diffusion coefficient K^s and the vertical gradient of the mean algal concentration P. Also, it is assumed that on the average the advective flux of chlorophyll a can be represented adequately by the quasi-steady state velocity components u and w.

Under these assumptions, a laterally-averaged equation for the concentration of plant chlorophyll $P(x,z,t)$ can be written as

$$P_t = \frac{1}{b}(bK^s P_z)_z - \frac{1}{b}[(buP)_x + (bwP)_z + (bw_g P)_z] + P_p(x,z,t)\,P - g_p H \quad (46)$$

where w_g is a representative vertical sinking speed of algal cells, P_p is the net specific production rate, g_p is the specific grazing rate, and H is the herbivore concentration.

In principle, Eq.(46) is to be solved in a specified space-time domain, subject to appropriate boundary conditions and an initial condition. The relevant space domain in the present instance is defined by

$$\{0 \le z \le L; \quad -10\ km \le x \le +80\ km\},$$

where L is 30 m. The bounds on x correspond to the mid-channel distances from Station 1 to Blake Island and the southern tip of Whidbey Island, respectively. The time domain is April 15 through June 30 for spring of 1966 and April 25 through May 30 for spring of 1967. The starting dates are chosen so as to be near the beginning of daily observations and to lie well within a time period when algal blooms were absent.

The boundary condition at the free surface requires that the flux of phytoplankton is zero:

$$-K^s P_z + w_g P = 0, \quad (47)$$

An appropriate boundary condition at depth is suggested by the observation that a low-level concentration of phytoplankton is maintained by the advection of cells into the basin with salt water intrusion. The deep chlorophyll concentration was assigned an average value for the observation period:

$$P = 1.5 \text{ mg Chl } a/m^3 \text{ at } z = 30 \text{ m}. \tag{48}$$

Boundary conditions at $x = -10$ km and +20 km could be specified on the basis of observations (see, e.g., Munson, 1970) that longitudinal gradients at the ends of the central basin segment are small on the average. In fact, a numerical study of the three-dimensional (x,z,t) problem was performed with such conditions. As expected from field observations, a slight relative increase in pigment was predicted in the down-inlet direction, but the chlorophyll distributions with depth were similar at all stations along the inlet axis. Since calculated phytoplankton concentrations at the central station differed by only a few percent from those predicted by a simpler, more economical two-dimensional (depth-time) model, the latter was subsequently used in the investigation. Thus, the x-derivative of P was assumed negligible throughout the length of the inlet segment, and the original three-dimensional problem was transformed to a two-dimensional one. Boundary conditions (47) and (48) are still applicable, and the two-dimensional analogue of Eq. (46) was solved for the two springtime intervals of 75 days and 75 days in 1966 and 1967, respectively. Initial conditions for the two periods were the observed vertical profiles of chlorophyll *a* at Station 1 on April 15, 1966, and April 25, 1967. The starting profiles actually used in the computations were adjusted at depth to pass smoothly through the seasonal average concentration of 1.5 mg Chl a/m^3.

The coefficients K^z and ω are obtained from the similarity analysis summarized in Section 3. For the purpose of calculating the dynamical response of phytoplankton to changes in circulation, the salinity distribution and the non-tidal flow field were calculated daily in response to (usually modest) changes in cumulative runoff rate and in the intensity of turbulent mixing (as related to tides).

The net specific production rate P_n is a complicated function of several environmental variables and physiological parameters; the reader is referred

to the paper by Winter et al. (1975) for a full discussion of the specification of P_p and also of the grazing rate g_p. In an effort to avoid biasing the results of the simulation, somewhat traditional descriptions of photosynthetic processes were used in the model, except when the conventional formulation of a particular process was clearly inadequate and a better alternative could be identified. In any event, the paper by Winter et al. (1975) presents the relevant formulations including the dependence of the production rate on nutrient availability, underwater light intensity, and parameters such as the cellular carbon-to-chlorophyll ratio, the maximum specific photosynthetic rate, P_{max}, and the optimum light intensity I_{max}. So far as sinking of algal cells is concerned, it was assumed that the sinking speed was a fixed constant except during those episodes when cellular activity was expected to decline due to prolonged nitrate depletion; at which times the sinking rate was increased. Finally, a single grazing function, independent of size of the grazers, was applied to the herbivorous zooplankton.

The relationships among the various components of the model are depicted in the diagram in Fig. 28. The hydrographic and climatic inputs, which include runoff intensity, tidal range, and insolation, were supplied on a daily basis. Observed nitrate distributions and estimated herbivore concentrations were also provided each day, and, therefore, these variables act as "forcing functions" in much the same way as the environmental inputs. The several model parameters, such as P_{max}, I_{max}, K_s, g_p, S_w, algal density at depth, etc., play a somewhat different role, inasmuch as they are of the nature of input constants, most of which are fixed throughout the course of a calculation. The feedback shown in the model diagram between the phytoplankton concentration submodel and the submodel for underwater light intensity is a consequence of the effect of self-shading on water transparency. Feedback also occurs between the phytoplankton submodel and the grazing submodel due to the dependence of the herbivore ration upon food concentration.

The numerical integrations carried out with the "best available" functional forms and parameter values were referred to as "standard runs" and were used in fact as standards for comparison with experimental simulations. In considering the standard run results, it is important to note that because the model in its present form does not include explicitly the effects of sustained winds, it was

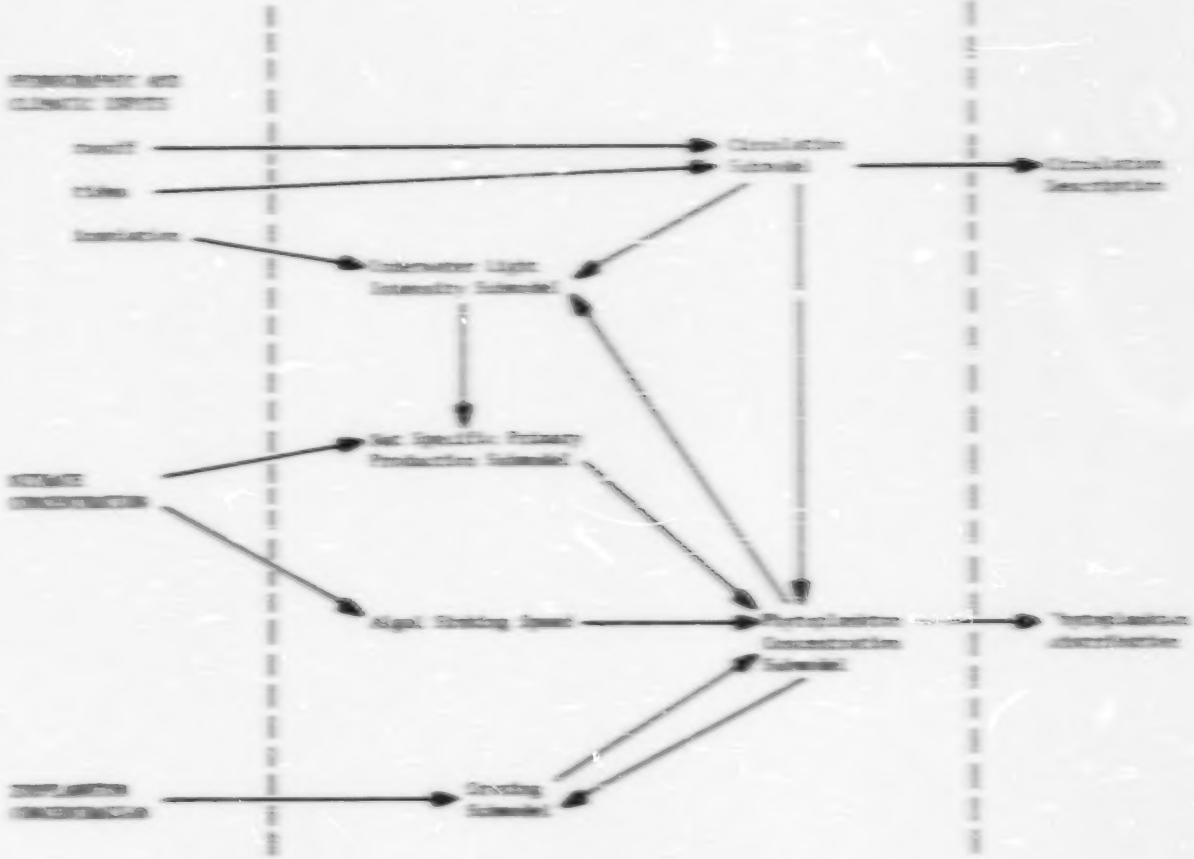

Fig. 38. Flow diagram of numerical model showing relationship among the several components of the model.

necessary to perform the 1966 computation in two stages. In an open inlet, such as Puget Sound, occasional episodes of strong, persistent winds will drastically retard or accelerate seaward advection in the upper zone, simultaneously altering its density structure and phytoplankton content. Such an occurrence is exemplified by an abrupt change in surface salinity around mid-May 1966. Beginning on 12 May, an episode of high runoff due to snow melt was followed immediately by sustained strong southerly winds which rapidly moved the relatively fresh surface water to the north and, at the same time, removed from the central basin the algal blooms which had previously been extant in the surface zone. The reduction of the freshwater fraction in the surface zone was accompanied by upwelling of saline water from depth and the occurrence of low rates of specific algal production. Therefore, the calculation for 1966, which began on April 15, was terminated on 15 May, which was the third consecutive day on which the average wind speed was near or exceeded 10 knots. The algal density was reset at 1.0 mg Chl a/m^3 near the surface, in accord with observations, and the computation continued without further interruption to the end of June. Although there were episodes of winds during the 1967 period, they were of shorter duration and lesser intensity, and, as a consequence, the entire calculation for 1967 was performed without interruption.

The day-to-day variations of the computed Secchi disk depth and the integrated chlorophyll values of the standard computer runs are shown together with the observed values for the springtime periods of 1966 and 1967 in Figs. 29 and 30. The comparison of the computed and observed results indicates that the model reproduces satisfactorily not only the general pigment level but also many of the details of the springtime phytoplankton dynamics in both years. Moreover, the explanations for the periods of divergence between calculated and observed values are set forth in the paper by Winter et al.(1975). The reader is also referred to that paper for a discussion of various numerical experiments which were performed and the conclusions to be drawn from each one.

Observed and calculated (standard run) depth distributions of chlorophyll before, during, and after the first intense algal bloom in 1966 are compared in Fig. 31. It is evident that the near-surface concentrations are fairly well represented, although the predicted profile is smoother than that inferred from the

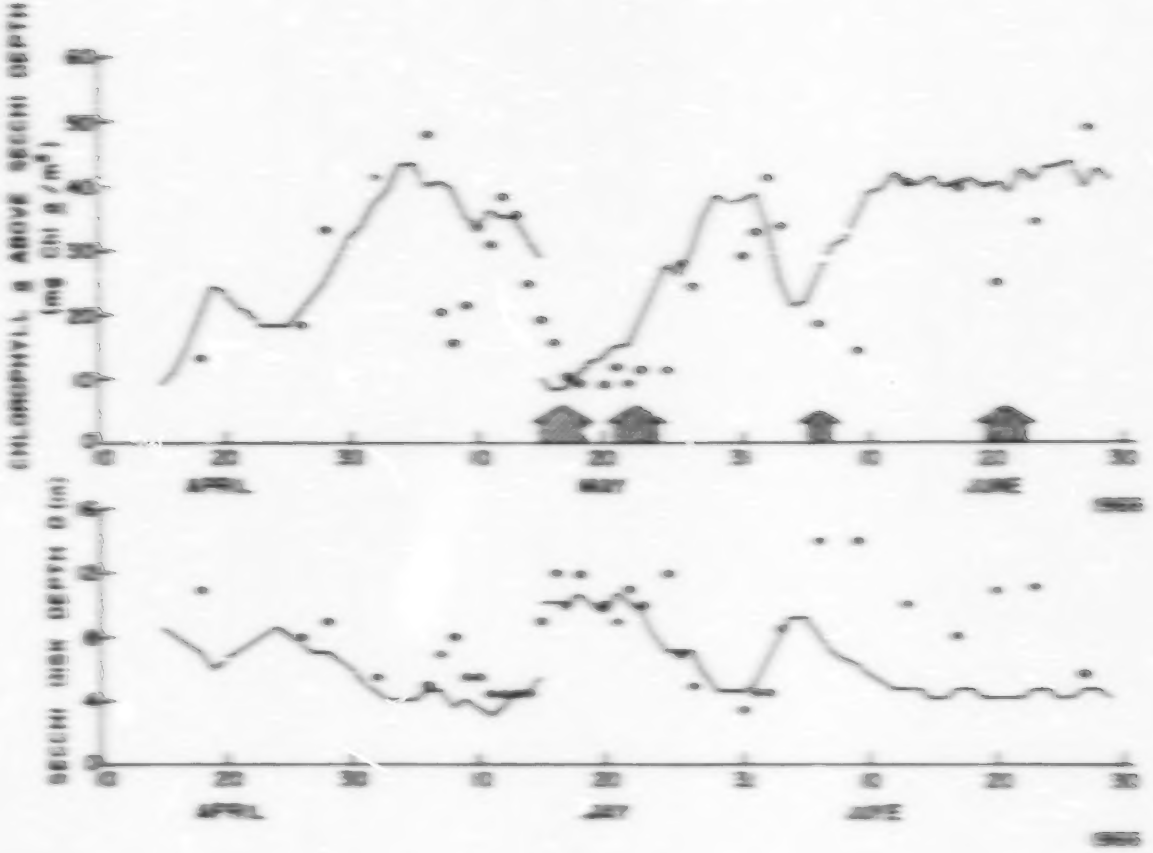

Fig. 28. Comparison of measured and calculated integrated chlorophyll a from surface to Secchi disk depth and Secchi disk depth at Station 1 in Puget Sound, April to June 1966; arrows indicate ecdiage of periods of rapidly rising salinity in brackish zone.

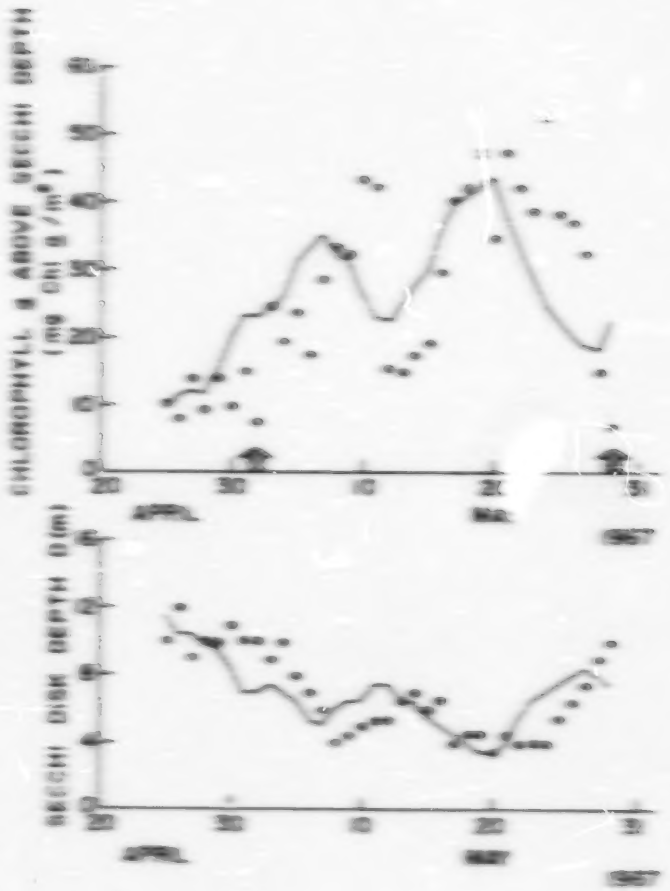

Fig. 38. Comparison of measured and calculated integrated chlorophyll a from surface to Secchi disk depth and Secchi disk depth at Station 1 in Puget Sound, April and May 1967.

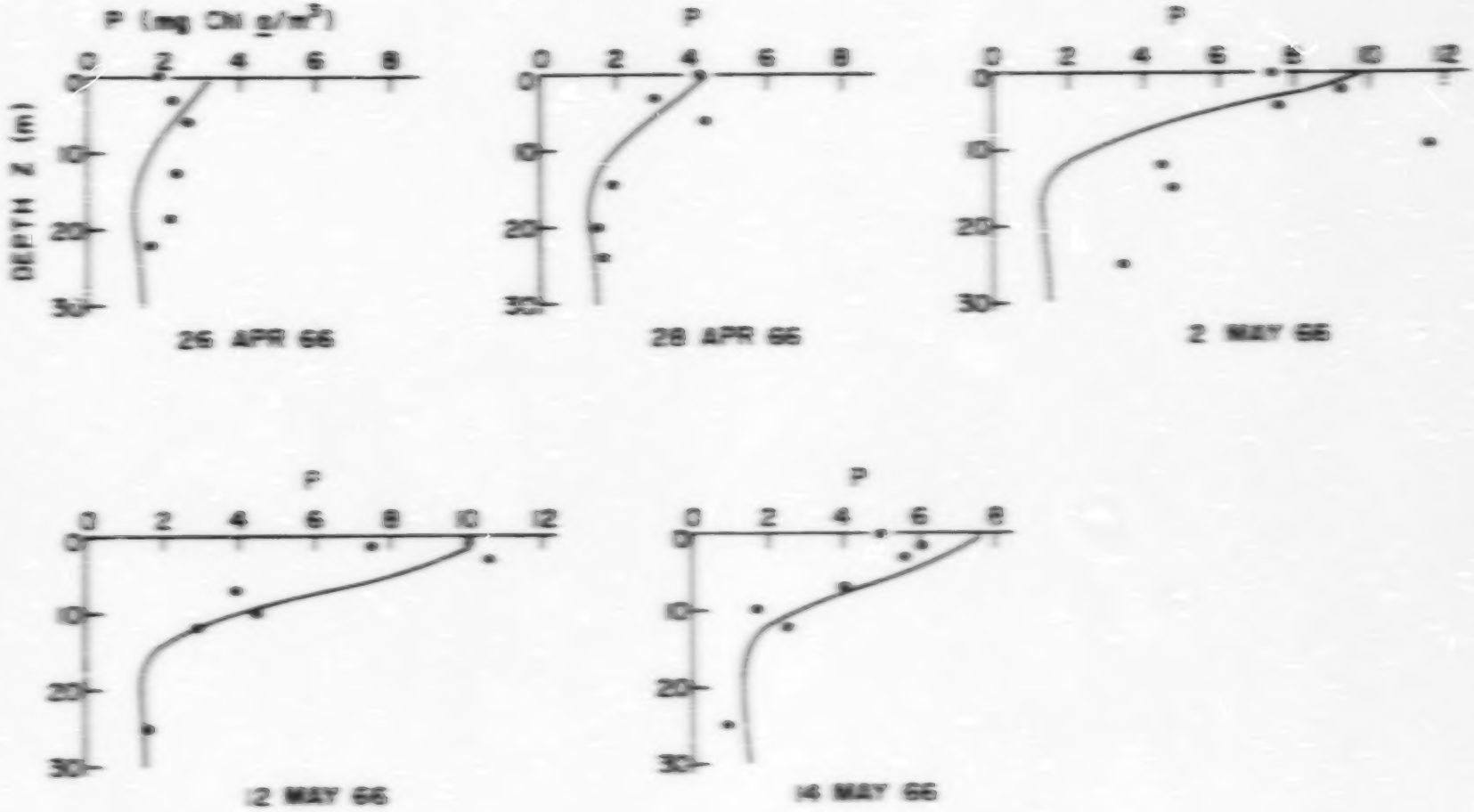

Fig. 11. Comparison of measured and calculated chlorophyll *a* concentrations as functions of depth at Station 1 before, during, and after algal bloom in 1966; dashed lines indicate estimates of 1% light depths.

observations. It is also apparent that the model fails to reproduce concentrations near and below the euphotic zone when the bloom is in progress. This particular shortcoming was anticipated in view of the crudeness of the boundary condition at depth. In addition, minimal phytoplankton concentrations are predicted by the model below the halocline in the region around 30 m depth, possibly as a result of low net *in situ* production, combined with an underestimate of mixing, resulting in insufficient downward transport of near-surface algal material and upwelled seed stock from depth.

In summary, the calculations of the standard run reproduced most of the general features of data acquired during the springtime cruises in 1966 and 1967. The results of the standard runs and the numerical experiments with the model confirm the existence of a close relationship between the circulation and the physical and chemical properties of the water, climatic (light) conditions, and the level of primary production in Puget Sound. The model is general enough to be applicable to other deep temperate inlets where the general constraints on the physical submodel are satisfied and where nutrient exhaustion is not a major feature. Incorporation of nutrient regeneration by zooplankton would be necessary in the Strait of Georgia and in inlets subsidiary to the central basin of Puget Sound where nitrate levels are low over prolonged periods of time.

The model study lends further support to the notion that gravitational convection supplies the euphotic zone with algal seed stock from depth and replenishes exhausted supplied of essential nutrients during vigorous flowering. A complete quantitative verification of these hypotheses is somewhat beyond the present state-of-the-art, since it would require the development of fjord circulation models which include the influence of bathymetry (especially sills), the effect of winds, and changing hydrographic conditions in external source waters. Nevertheless, various results of the model computations, such as the flux component profiles shown in Fig. 32, indicate that the high productivity of Puget Sound is due to strong, persistent upwelling of nutrients and algal cells from depth. During the spring and early summer, the quantity and quality of freshwater runoff in the central basin is apparently such as to maintain moderately intense gravitational convection without producing an excessively turbid brackish surface layer.

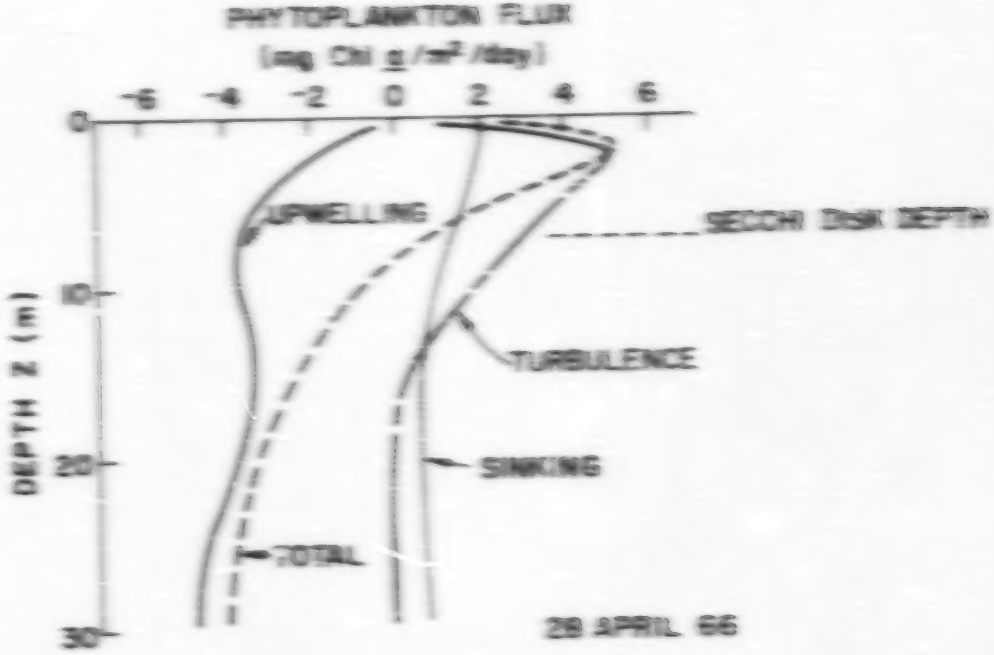

Fig. 32. Depth variation of algal flux due to turbulent mixing, upwelling, and sinking for standard run at noon on 28 April 1966.

In contrast with the situation in the open sea, the mixing processes in the main channel of Puget Sound do not create a deep mixed layer within which primary production is light-limited. Instead, algal growth in the central basin is limited by a combination of hydrodynamic factors (as illustrated in Fig. 32) and modulation of the underwater light intensity by self-shading and by inorganic particulates. On occasions of sustained winds, standing stock is limited by relatively short residence times determined by horizontal advection. Evidently, the late occurrence of spring blooms in deep inlets like Puget Sound is not explainable in terms of the critical depth concept.

In the central basin of the Sound, several consecutive days of bright sunshine are sufficient to promote massive development of phytoplankton. Given the right combination of weather, water stratification, and flushing characteristics in the upper brackish zone, blooms might also occur earlier in the year, but apparently these instances are somewhat uncommon and have not been observed during 1964 and 1965. As noted above, horizontal advection by sustained winds will remove blooms from the central basin; prolonged nitrate depletion and a succession of cloudy days will discourage vigorous growth and will cause a bloom to decline in intensity. By means of numerical experiments, it was demonstrated that the effects of grazing by herbivorous zooplankton and cellular sinking are of secondary importance. Because of the rather rare occurrence of nutrient limitation during the spring and the light limitation that prevails during the fall and winter months, nutrient addition from sewage treatment plants is not likely to change the level of primary production in the main channel significantly.

SECTION 6

REFERENCES

Barlow, J.P., 1956. Spring changes in phytoplankton abundance in a deep estuary, Hood Canal, Washington. Journal of Marine Research 17, 53-67.

Bowden, K.F., and R.H. Gilligan, 1971. Characteristic features of estuarine circulation as represented in the Mersey estuary. Limnology and Oceanography 16, 490-502.

Cannon, G.A., and N.P. Laird, 1972. Observations of currents and water properties in Puget Sound, 1972. NOAA Technical Report ERL 247-PMEL 13, National Oceanic and Atmospheric Administration, Boulder, Colorado.

Dyer, K.R., 1973. Estuaries: A Physical Introduction. Chapter 5. John Wiley and Sons, New York.

Fretheretshauser, M.A., and A.C. Duxbury, 1972. A water budget study of Puget Sound and its subregions. Limnology and Oceanography 17(3), 237-247.

Gade, H.G., 1968. Horizontal and vertical exchanges and diffusion in the water masses of the Oslo Fjord. HeligolNnder Wissenschaftliche 17, 462-475.

Kullenberg, G., 1971. Vertical diffusion in shallow waters. Tellus 23, 129-135.

McAlister, W.B., M. Mattray, Jr., and C.A. Barnes, 1959. The dynamics of a fjord estuary: Silver Bay, Alaska. Department of Oceanography Technical Report No. 62. University of Washington, Seattle, Washington.

Munson, R.E., 1970. The horizontal distribution of phytoplankton in a bloom in Puget Sound during May, 1969. 13 pp. Non-thesis masters report, Department of Oceanography, University of Washington, Seattle, Washington.

Paquette, R.G., and C.A. Barnes, 1951. Measurement of tidal currents in Puget Sound. Department of Oceanography Technical Report No. 6. University of Washington, Seattle, Washington.

Pearson, C.E., and D.F. Winter, 1976. A numerical model of steady two-zone flow in deep stratified inlets. Interim report on Grant No. R801320 with the Environmental Protection Agency, National Environmental Research Center, Corvallis, Oregon.

Pickard, G.L., 1961. Oceanographic features of inlets in the British Columbia mainland coast. Journal of the Fisheries Research Board of Canada 18, 907-999.

Pickard, G.L., 1971. Some physical oceanographic features of inlets of Chile. Journal of Fisheries Research Control Board of Canada 28, 1077-1106.

Pickard, G.L., and K. Rodgers, 1959. Current measurements in Knight Inlet, British Columbia. Journal of the Fisheries Research Board of Canada 16, 635-678.

Rattray, M., Jr., 1967. Some aspects of the dynamics of circulation in fjords. In, Estuaries (Lauff, G.H., ed.). American Association for the Advancement of Science, Washington, D.C., pp. 52-62.

Rattray, M., Jr., and J.H. Lincoln, 1955. Operating characteristics of an oceanographic model of Puget Sound, Trans. AGU, 36(2), 251.

Trites, R.W., 1955. A study of the oceanographic structure in British Columbia inlets and some of the determining factors. Ph.D. thesis, University of British Columbia, Vancouver, British Columbia.

Tully, J.P., 1949. Oceanography and prediction of pulp mill pollution in Alberni Inlet. Bulletin Fisheries Research Board of Canada, No. 83.

Winter, D.F., 1973. A similarity solution for steady-state gravitational circulation in fjords. Estuarine and Coastal Marine Science 1, 387-400.

Winter, D.F., K. Banse, and G.C. Anderson, 1975. The dynamics of phytoplankton blooms in Puget Sound, a fjord in the northwestern United States. Marine Biology 29, 139-176.

Winter, D.F., and C.E. Pearson, 1976. Computation of steady circulation in stratified fjords. Proceedings Fifth Technical Conference, Estuaries of the Pacific Northwest. April 1 and 2, 1976. Oregon State University, Corvallis, Oregon.

SECTION 7

PUBLICATIONS AND TECHNICAL MEMORANDA

RESULTING FROM EPA GRANT NO. R-801320 (TO APRIL 1976)

1. Lam, R. and J. Lincoln 1975. Model Study of Surface Tidal Currents in Puget Sound. Project Report on EPA Grant No. R801320. Ref. No. M75-109, October 1975. Department of Oceanography, University of Washington, Seattle.

2. Lincoln, J. and R. Lam 1975. A Hydraulic Model Study of Dye-Stream Dispersal Characteristics in Some Parts of Puget Sound. Project Report on EPA Grant No. R801320. Ref. No. M75-108, October 1975. Department of Oceanography, University of Washington, Seattle.

3. Pearson, C. E. and D. F. Winter 1974. A Numerical Study of Time-Dependent Shallow Water Motion in Stratified Inlets. Interim Report on EPA Grant No. R801320. Department of Oceanography, University of Washington, Seattle.

4. Pearson, C. E. and D. F. Winter 1975. Analysis of Stratified Inlet Flow by the Method of Weighted Residuals. Symposium on Modeling of Transport Mechanisms in Oceans and Lakes. Canada Centre for Inland Waters, Burlington, Ontario. October 6-8, 1975.

5. Pearson, C. E. and D. F. Winter 1976. Computation of Tidal Flow in Well-Mixed Estuaries. *Journal of the Hydraulics Division, ASCE, Vol.* 102, No. HY3, p. 367-377.

6. Pearson, C. E. and D. F. Winter 1976. Summary of Efficient Computation of Tidal Currents in Estuaries. Proceedings of the Technical Conference on Estuaries of the Pacific Northwest. Oregon State University, p. 39-41.

7. Pearson, C. E. and D. F. Winter 1976. A numerical Model of Steady Two-Zone Flow in Deep Stratified Inlets. Interim Report on EPA Grant No. R801320. Department of Oceanography, University of Washington, Seattle.

8. Winter, D. F. 1973. A Similarity Solution for Steady-State Gravitational Circulation in Fjords. *Estuarine and Coastal Marine Science* 1:387-404.

9. Winter, D. F., K. Banse, and G. C. Anderson 1975. The Dynamics of Phytoplankton Blooms in Puget Sound, A Fjord in the Northwestern United States. *Marine Biology* 29:139-176.

10. Winter, D. F. and C. E. Pearson 1976. Computation of Steady Circulation in Stratified Fjords. Proceedings 5th Technical Conference on Estuaries of the Pacific Northwest. Oregon State University. p. 55-58.

11. Winter, D. F. and C. E. Pearson 1976. A Numerical Model of Time-Dependent Two-Zone Flow in Stratified Inlets. Interim Report on EPA Grant No. R801320. Department of Oceanography, University of Washington, Seattle.